



IJOER
RESEARCH JOURNAL

ISSN
2395-6992

International Journal of Engineering Research & Science

www.ijoer.com

www.adpublications.org

Volume-4! Issue-12! December, 2018 www.ijoer.com ! info@ijoer.com

Preface

We would like to present, with great pleasure, the inaugural volume-4, Issue-12, December 2018, of a scholarly journal, *International Journal of Engineering Research & Science*. This journal is part of the AD Publications series *in the field of Engineering, Mathematics, Physics, Chemistry and science Research Development*, and is devoted to the gamut of Engineering and Science issues, from theoretical aspects to application-dependent studies and the validation of emerging technologies.

This journal was envisioned and founded to represent the growing needs of Engineering and Science as an emerging and increasingly vital field, now widely recognized as an integral part of scientific and technical investigations. Its mission is to become a voice of the Engineering and Science community, addressing researchers and practitioners in below areas

Chemical Engineering	
Biomolecular Engineering	Materials Engineering
Molecular Engineering	Process Engineering
Corrosion Engineering	
Civil Engineering	
Environmental Engineering	Geotechnical Engineering
Structural Engineering	Mining Engineering
Transport Engineering	Water resources Engineering
Electrical Engineering	
Power System Engineering	Optical Engineering
Mechanical Engineering	
Acoustical Engineering	Manufacturing Engineering
Optomechanical Engineering	Thermal Engineering
Power plant Engineering	Energy Engineering
Sports Engineering	Vehicle Engineering
Software Engineering	
Computer-aided Engineering	Cryptographic Engineering
Teletraffic Engineering	Web Engineering
System Engineering	
Mathematics	
Arithmetic	Algebra
Number theory	Field theory and polynomials
Analysis	Combinatorics
Geometry and topology	Topology
Probability and Statistics	Computational Science
Physical Science	Operational Research
Physics	
Nuclear and particle physics	Atomic, molecular, and optical physics
Condensed matter physics	Astrophysics
Applied Physics	Modern physics
Philosophy	Core theories

Chemistry	
Analytical chemistry	Biochemistry
Inorganic chemistry	Materials chemistry
Neurochemistry	Nuclear chemistry
Organic chemistry	Physical chemistry
Other Engineering Areas	
Aerospace Engineering	Agricultural Engineering
Applied Engineering	Biomedical Engineering
Biological Engineering	Building services Engineering
Energy Engineering	Railway Engineering
Industrial Engineering	Mechatronics Engineering
Management Engineering	Military Engineering
Petroleum Engineering	Nuclear Engineering
Textile Engineering	Nano Engineering
Algorithm and Computational Complexity	Artificial Intelligence
Electronics & Communication Engineering	Image Processing
Information Retrieval	Low Power VLSI Design
Neural Networks	Plastic Engineering

Each article in this issue provides an example of a concrete industrial application or a case study of the presented methodology to amplify the impact of the contribution. We are very thankful to everybody within that community who supported the idea of creating a new Research with IJOER. We are certain that this issue will be followed by many others, reporting new developments in the Engineering and Science field. This issue would not have been possible without the great support of the Reviewer, Editorial Board members and also with our Advisory Board Members, and we would like to express our sincere thanks to all of them. We would also like to express our gratitude to the editorial staff of AD Publications, who supported us at every stage of the project. It is our hope that this fine collection of articles will be a valuable resource for *IJOER* readers and will stimulate further research into the vibrant area of Engineering and Science Research.



Mukesh Arora
(Chief Editor)

Board Members

Mukesh Arora(Editor-in-Chief)

BE(Electronics & Communication), M.Tech(Digital Communication), currently serving as Assistant Professor in the Department of ECE.

Prof. Dr. Fabricio Moraes de Almeida

Professor of Doctoral and Master of Regional Development and Environment - Federal University of Rondonia.

Prof.S.Balamurugan

Department of Information Technology, Kalaignar Karunanidhi Institute of Technology, Coimbatore, Tamilnadu, India.

Dr. Omar Abed Elkareem Abu Arqub

Department of Mathematics, Faculty of Science, Al Balqa Applied University, Salt Campus, Salt, Jordan, He received PhD and Msc. in Applied Mathematics, The University of Jordan, Jordan.

Dr. AKPOJARO Jackson

Associate Professor/HOD, Department of Mathematical and Physical Sciences, Samuel Adegboyega University, Ogwa, Edo State.

Dr. Ajoy Chakraborty

Ph.D.(IIT Kharagpur) working as Professor in the department of Electronics & Electrical Communication Engineering in IIT Kharagpur since 1977.

Dr. Ukar W.Soelistijo

Ph D , Mineral and Energy Resource Economics, West Virginia State University, USA, 1984, Retired from the post of Senior Researcher, Mineral and Coal Technology R&D Center, Agency for Energy and Mineral Research, Ministry of Energy and Mineral Resources, Indonesia.

Dr. Samy Khalaf Allah Ibrahim

PhD of Irrigation &Hydraulics Engineering, 01/2012 under the title of: "Groundwater Management Under Different Development Plans In Farafra Oasis, Western Desert, Egypt".

Dr. Ahmet ÇİFCİ

Ph.D. in Electrical Engineering, Currently Serving as Head of Department, Burdur Mehmet Akif Ersoy University, Faculty of Engineering and Architecture, Department of Electrical Engineering (2015-...)

Dr. Heba Mahmoud Mohamed Afify

Ph.D degree of philosophy in Biomedical Engineering, Cairo University, Egypt worked as Assistant Professor at MTI University.

Dr. Aurora Angela Pisano

Ph.D. in Civil Engineering, Currently Serving as Associate Professor of Solid and Structural Mechanics (scientific discipline area nationally denoted as ICAR/08—"Scienza delle Costruzioni"), University Mediterranea of Reggio Calabria, Italy.

Dr. Faizullah Mahar

Associate Professor in Department of Electrical Engineering, Balochistan University Engineering & Technology Khuzdar. He is PhD (Electronic Engineering) from IQRA University, Defense View, Karachi, Pakistan.

Dr. S. Kannadhasan

Ph.D (Smart Antennas), M.E (Communication Systems), M.B.A (Human Resources).

Dr. Christo Ananth

Ph.D. Co-operative Networks, M.E. Applied Electronics, B.E Electronics & Communication Engineering Working as Associate Professor, Lecturer and Faculty Advisor/ Department of Electronics & Communication Engineering in Francis Xavier Engineering College, Tirunelveli.

Dr. S.R.Boselin Prabhu

Ph.D, Wireless Sensor Networks, M.E. Network Engineering, Excellent Professional Achievement Award Winner from Society of Professional Engineers Biography Included in Marquis Who's Who in the World (Academic Year 2015 and 2016). Currently Serving as Assistant Professor in the department of ECE in SVS College of Engineering, Coimbatore.

Dr. Maheshwar Shrestha

Postdoctoral Research Fellow in DEPT. OF ELE ENGG & COMP SCI, SDSU, Brookings, SD
Ph.D, M.Sc. in Electrical Engineering from SOUTH DAKOTA STATE UNIVERSITY, Brookings, SD.

Zairi Ismael Rizman

Senior Lecturer, Faculty of Electrical Engineering, Universiti Teknologi MARA (UiTM) (Terengganu) Malaysia
Master (Science) in Microelectronics (2005), Universiti Kebangsaan Malaysia (UKM), Malaysia. Bachelor (Hons.) and Diploma in Electrical Engineering (Communication) (2002), UiTM Shah Alam, Malaysia

Dr. D. Amaranatha Reddy

Ph.D.(Postdoctoral Fellow,Pusan National University, South Korea), M.Sc., B.Sc. : Physics.

Dr. Dibya Prakash Rai

Post Doctoral Fellow (PDF), M.Sc.,B.Sc., Working as Assistant Professor in Department of Physics in Pachhungga University College, Mizoram, India.

Dr. Pankaj Kumar Pal

Ph.D R/S, ECE Deptt., IIT-Roorkee.

Dr. P. Thangam

BE(Computer Hardware & Software), ME(CSE), PhD in Information & Communication Engineering, currently serving as Associate Professor in the Department of Computer Science and Engineering of Coimbatore Institute of Engineering and Technology.

Dr. Pradeep K. Sharma

PhD., M.Phil, M.Sc, B.Sc, in Physics, MBA in System Management, Presently working as Provost and Associate Professor & Head of Department for Physics in University of Engineering & Management, Jaipur.

Dr. R. Devi Priya

Ph.D (CSE), Anna University Chennai in 2013, M.E, B.E (CSE) from Kongu Engineering College, currently working in the Department of Computer Science and Engineering in Kongu Engineering College, Tamil Nadu, India.

Dr. Sandeep

Post-doctoral fellow, Principal Investigator, Young Scientist Scheme Project (DST-SERB), Department of Physics, Mizoram University, Aizawl Mizoram, India- 796001.

Mr. Abilash

MTech in VLSI, BTech in Electronics & Telecommunication engineering through A.M.I.E.T.E from Central Electronics Engineering Research Institute (C.E.E.R.I) Pilani, Industrial Electronics from ATI-EPI Hyderabad, IEEE course in Mechatronics, CSHAM from Birla Institute Of Professional Studies.



Mr. Varun Shukla

M.Tech in ECE from RGPV (Awarded with silver Medal By President of India), Assistant Professor, Dept. of ECE, PSIT, Kanpur.

Mr. Shrikant Harle

Presently working as a Assistant Professor in Civil Engineering field of Prof. Ram Meghe College of Engineering and Management, Amravati. He was Senior Design Engineer (Larsen & Toubro Limited, India).

Table of Contents

S.No	Title	Page No.
1	<p>Composition Determination of Corrosion Products from Downhole Tubular of a Sour Gas Well Using new XRD and WDXRF Procedures and Configurations</p> <p>Authors: Shouwen Shen, Quanwen Liu, Qiwei Wang, Yousef M. Salim</p> <p> DOI: 10.5281/zenodo.2529355</p> <p> DIN Digital Identification Number: IJOER-DEC-2018-2</p>	01-07
2	<p>The optimal configuration of turbines location in a wind farm using a Genetic Algorithm</p> <p>Authors: DAOUDI Mohammed, ELKHOZAI Elmostapha</p> <p> DOI: 10.5281/zenodo.2529357</p> <p> DIN Digital Identification Number: IJOER-DEC-2018-3</p>	08-18
3	<p>Improvement of Biometric Authentication System Applying Fingerprint</p> <p>Authors: Fatamatuz Ayasa Khan</p> <p> DOI: 10.5281/zenodo.2529363</p> <p> DIN Digital Identification Number: IJOER-DEC-2018-5</p>	19-26
4	<p>Kalman Filter Based Approach of a signal by removing ICI for OFDM Channel</p> <p>Authors: Lokesh Kumar</p> <p> DOI: 10.5281/zenodo.2590890</p> <p> DIN Digital Identification Number: IJOER-DEC-2018-8</p>	27-31

Composition Determination of Corrosion Products from Downhole Tubular of a Sour Gas Well Using new XRD and WDXRF Procedures and Configurations

Shouwen Shen¹, Quanwen Liu^{2*}, Qiwei Wang³, Yousef M. Salim⁴

^{1,3}Research & Development Center, Saudi Aramco, Saudi Arabia

²School of Petroleum Engineering, Guangdong University of Petrochemical Technology, China

⁴South Area Production Engineering Department, Saudi Aramco, Saudi Arabia

*Corresponding author; Email: quanwenliu64@yahoo.com




Abstract—Corrosion study and control of downhole tubing and casing are critical for the economical and safe operation of oil and gas wells. Chemical composition investigation of corrosion products plays a key role in the identification of the corrosion mechanism and the determination of its root cause. In this study, the analytical techniques of X-ray diffraction (XRD) and wavelength dispersive X-ray fluorescence (WDXRF) spectrometry were used to determine the chemical composition of corrosion products formed on the pulled-out-of-hole (POOH) flow coupling and full joints of a sour gas well in Saudi Arabia. The samples were in the form of metal cuts and could not be prepared with the routine method for XRD and WDXRF analysis. These unconventional samples were handled using an adapted XRD configuration: X-ray point focus rather than line focus and an open eulerian cradle. With the new setup, XRD phase identification and quantification were successfully performed. It was found that the outer diameter surface of the pulled flow coupling and full joints consisted mainly of iron oxides whereas the inner diameter surface consisted mainly of iron sulfides. The XRD findings were further confirmed by WDXRF analysis. The findings suggested that the corrosion products were formed under different conditions.

Keywords—Corrosion products, iron oxide, iron sulfide, XRD analysis, WDXRF analysis.

I. INTRODUCTION

Corrosion is the destructive attack of a material by reaction with its environment^[1] and a natural potential hazard associated with oil and gas production and transportation facilities.^[2] Almost any aqueous environment can promote corrosion, which occurs under numerous complex conditions in oil and gas production, processing, and pipelines systems.^[3] Crude oil and natural gas can carry various high-impurity products which are inherently corrosive. In the case of oil and gas well, such highly corrosive media are carbon dioxide, hydrogen sulfide, and free water.^[4] Continual extraction of carbon dioxide, hydrogen sulfide and free water through oil and gas components can over time make the internal surfaces of these components to suffer from corrosion effects. The lines and their component would undergo material degradations with the varying conditions of the well due to changes in fluid compositions, souring of wells over the period, and changes in operating conditions of the pressures and temperatures. This material degradation results in the loss of mechanical properties like strength, ductility, and so on. This leads to loss of materials, reduction in thickness, and at times ultimate failure.^[5] Therefore, study and control of downhole tubing and casing are critical for the economic and safe operation of oil and gas wells. In this case study, a sour gas producing well in Saudi Arabia was selected for the investigation. This well was put on producing in 2009 and the production has declined over time. Four metal cuts samples were taken out from the downhole tubular (**Table 1**) and the corrosion products were analyzed. In order to investigate the exact composition and nature of the corrosion products, the analytical techniques of X-ray diffraction (XRD) and wavelength dispersive X-ray fluorescence (WDXRF) spectrometry were used.

TABLE 1
SAMPLE INFORMATION

Sample #	#1	#2	#3	#4
Description	Flow coupling inner side	Flow coupling outer side	Joint cut inner side	Joint cut outer side
Picture				

II. EXPERIMENTAL

2.1 Challenges faced

For routine composition analysis using XRD and WDXRF techniques, the samples to be analyzed should be in dry powder status. However, the samples in this study were in the form of metal cuts and could not be ground into powder. Special handling procedures and new instrumental configurations were needed.

2.2 Solution with WDXRF Analysis

X-ray fluorescence spectrometry (XRF) is an analytical technique to determine the elemental composition of various materials. XRF has the advantage of being non-destructive, multi-elemental, fast and cost-effective.^[6, 7] XRF technique can be categorized into two classes: energy dispersive X-ray fluorescence (EDXRF) and wavelength dispersive X-ray fluorescence (WDXRF) spectrometry. The elements that can be analyzed and their detection levels mainly depend on the spectrometer system used. The elemental range for EDXRF goes from sodium (Na) to uranium (U). For WDXRF it is even wider, from beryllium (Be) to uranium (U). The concentration range goes from part per million (ppm) levels to 100%. For routine elemental analysis, the analyzed samples will be ground into powder and pressed into pellet or melt into fusion beads. In this study, all samples were directly put in a special sample holder and measured as-received (metal cuts) in helium atmosphere rather than in vacuum condition. WDXRF data were obtained using Ominion standardless method for elemental composition determination semi-quantitatively with PANalytical Advanced Axios spectrometer.

TABLE 2
WDXRF RESULTS OF METAL CUTS FROM A DOWNHOLE TUBULAR

Element	Flow Coupling Cut		Joint Cut	
	Inner Side (Wt.%)	Outer Side (Wt.%)	Inner Side (Wt.%)	Outer Side (Wt.%)
Fe	70.2	59.5	56.9	53.8
Cr	12.4	3.9	10.8	2.6
S	7.2	0.2	12.6	0.4
Ni	4.0	0.9	4.3	0.4
Mo	1.8	1.2	1.6	1.1
Si	0.6	0.5	0.5	0.5
Al	0.5	0.4	0.3	0.3
Mg	0.5	0.4	0.5	0.5
Ca	0.2	0.6	0.6	8.4
Mn	0.1	0.1	0.2	0.2
Na	0.1	0.1	0.1	0.1
Ba		-	8.5	-

2.3 Solution with XRD Analysis

XRD is a non-destructive technique for analyzing a wide range of materials, including metals, minerals, polymers, catalysts, plastics, pharmaceuticals, thin-film coatings, ceramics, solar cells and semiconductors.^[6, 7] Therefore, XRD has become an indispensable method for materials investigation, characterization and quality control. In this study, XRD analysis was performed on four samples collected from the downhole tubular of a sour gas well. As all samples were in form of metal cuts and they could not be ground into powder with the routine method for XRD analysis. A special XRD configuration (X-Ray point focus rather than line focus) and new setup (using Open Eulerian Cradle) were adapted in order to handle these unconventional samples. With the new setup, XRD phase identification and quantification were successfully performed. The XRD patterns of the metal cuts samples were measured as received using a PANalytical X'Pert PRO PW3050/60 diffractometer (CuK α radiation generated at 45 kV and 40 mA) equipped with an automatic divergence slit, irradiated length of 15 mm, receiving slit size of 0.3 mm, single Xenon detector and an open eulerian cradle with manual Z translation stage for sample directly mounting. The samples were measured from 10 ° to 95 ° 2 θ with a step size of 0.02 °, scan step time 1s. To identify the phases present in the samples, the XRD patterns of the samples were compared with every calculated pattern in the Powder Diffraction File (PDF) database from the International Center for Diffraction Data (ICDD). Using the search-match capabilities of XRD software JADE 9.1+ and the ICDD-PDF database, all phases present in the samples were identified. The quantification of the data was performed by using the Rietveld refinement method.

TABLE 3
XRD RESULTS OF METAL CUTS FROM A DOWNHOLE TUBULAR

Compound	Flow Coupling Cut		Joint Cut	
	Inner Side (Wt.%)	Outer Side (Wt.%)	Inner Side (Wt.%)	Outer Side (Wt.%)
Iron-Fe	98	-	18	-
Troilite-FeS	2	-	-	-
Magnetite-Fe ₃ O ₄	-	99	2	21
Hematite-Fe ₂ O ₃	-	1	-	63
Pyrite-FeS ₂	-	-	40	-
Pyrrhotite-Fe _{1-x} S	-	-	18	-
Barite-BaSO ₄	-	-	22	-
Aragonite-CaCO ₃	-	-	-	16

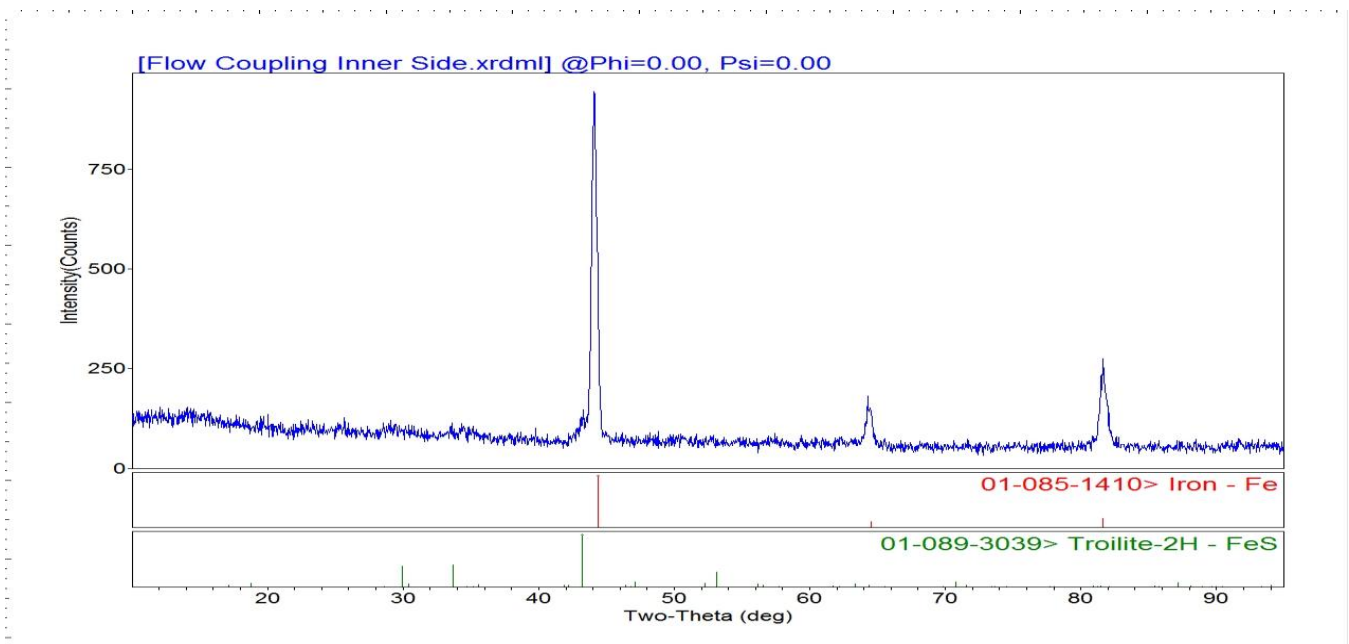


FIG. 1 XRD Pattern of Flow Coupling Inner Side

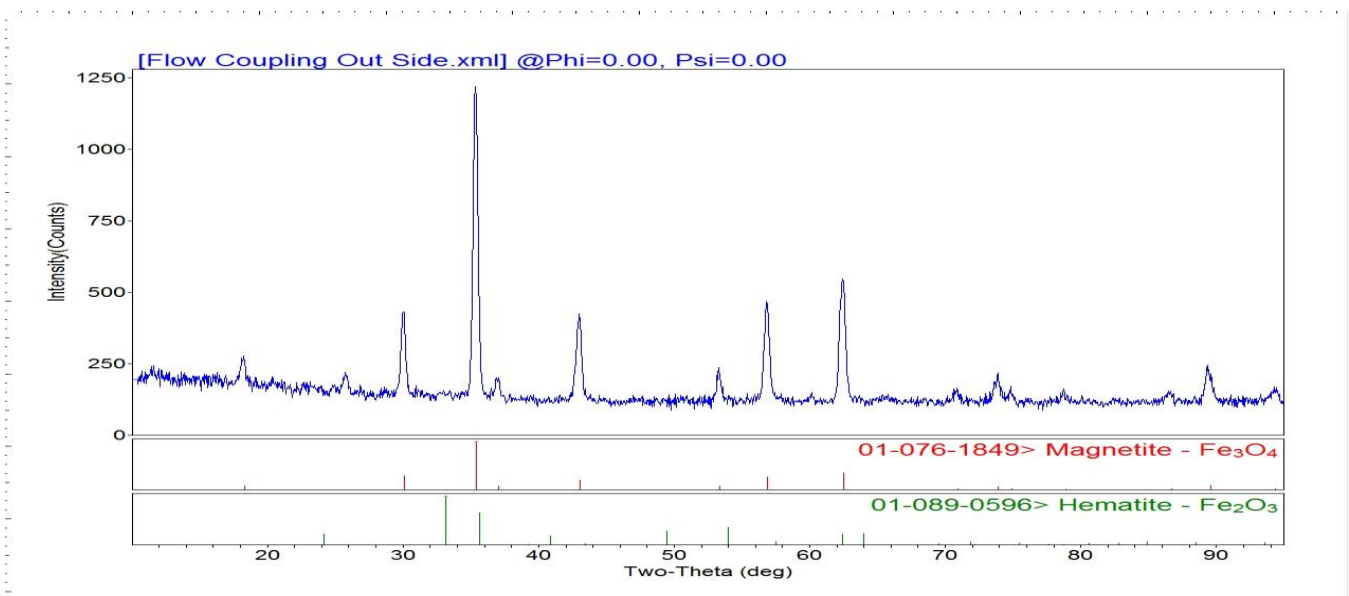


FIG. 2 XRD Pattern of Flow Coupling Out Side

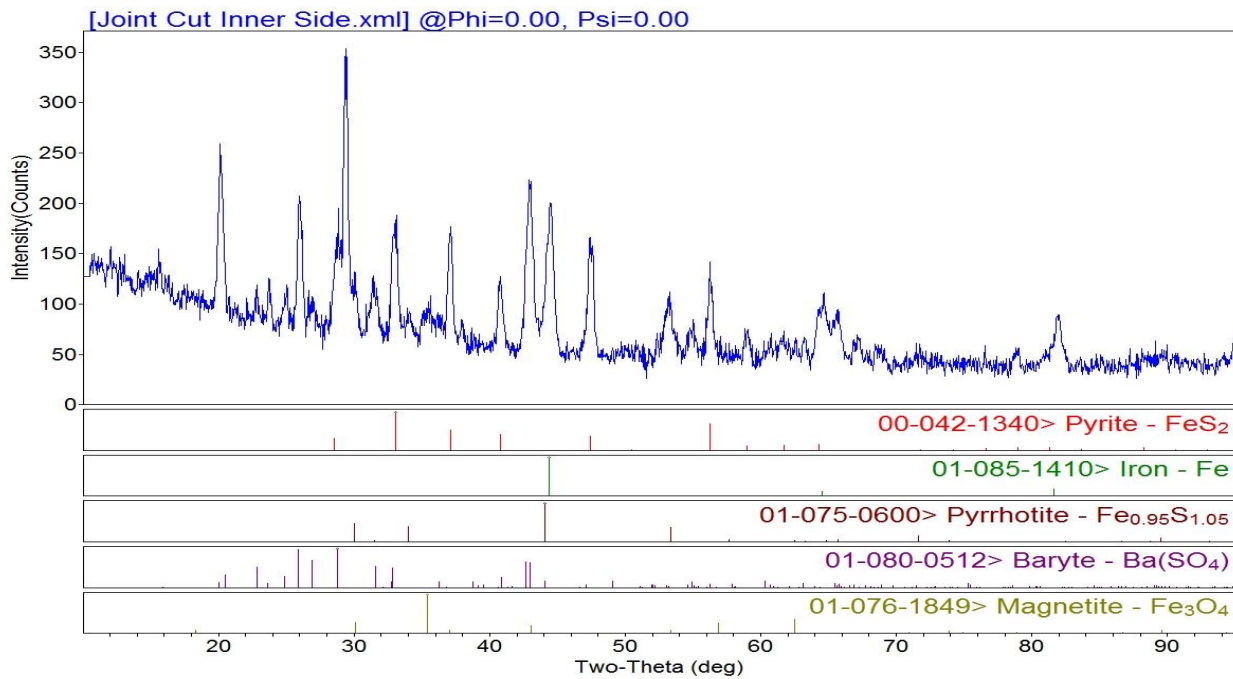


FIG. 3 XRD Pattern of Joint Cut Inner Side

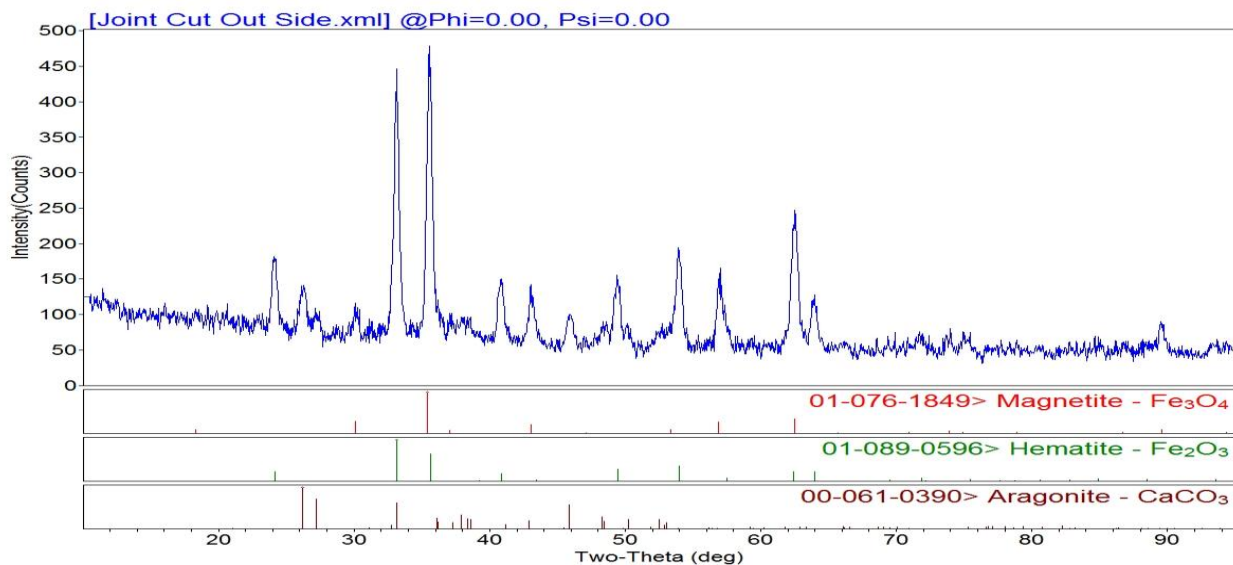


FIG. 4 XRD Pattern of Joint Cut Out Side

III. RESULTS AND DISCUSSION

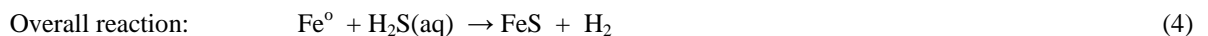
WDXRF results listed in **Table 2** indicate that iron (Fe) is the major element with an average of 60.1% (53.8% to 70.2%). The minor elements are chromium (Cr) with an average of 7.4% (2.6% to 12.4%) and sulfur (S) with an average of 5.1% (0.2% to 12.6%). Other elements such as Ni, Mo, Si, Al, Mg, Ca, Mn, Na, and Ba are also reported in small amounts. The XRD results of the identified compounds are listed in **Table 3** (relative approximate values, normalized to 100%) and the XRD patterns with identified compound references are illustrated in **Fig.1-4**. XRD results showed that the samples consisted mainly of corrosion products in form of magnetite- Fe_3O_4 , hematite- Fe_2O_3 , pyrite- FeS_2 , and pyrrhotite- Fe_{1-x}S with appreciable amounts of scale deposits in form of aragonite- CaCO_3 and barite- BaSO_4 . The original material of iron-Fe was also identified in the inner side samples. XRD results didn't show any chromium (Cr) containing compounds whereas WDXRF analysis

showed the samples contained chromium (Cr) with an average of 7.4% (2.6% to 12.4%). The reason is that Cr and other metal elements such as Ni and Mo etc. can replace Fe partially in iron oxides and iron sulfides. The findings revealed that the corrosion products of the tubular inner side were mainly iron sulfides whereas the corrosion products of the tubular outer side were mainly iron oxides, which indicated they were formed in different conditions. The inner side was exposed to high H₂S fluid and the outer side was in contact with packer fluid which contains no H₂S. Iron oxides usually form under oxidized conditions where dissolved iron is in the form of ferric state. The iron oxides identified in this study could be formed due to residual dissolved oxygen in packer fluid. At high temperatures, iron oxides can also be formed by the oxidation of ferrous iron (Fe²⁺) by H₂O in the absence of H₂S:^[8]



The formation of iron sulfides requires a strictly reducing environment. In fact, iron oxides are unstable in the presence of H₂S and can be quickly converted into iron sulfides.^[9,10]

It is reasonable that the inner side samples had the corrosion products of iron sulfides as the samples were collected from a sour gas well and H₂S reaction with steel (iron-Fe) tubular occurred in the sour gas flow system. Mild steel is susceptible to H₂S attack and iron sulfide is formed as a reaction by-product. This process has been extensively investigated and well documented.^[11-13] The established reactions between iron and H₂S are as follows:



Where FeS represents the iron sulfide by-products formed. Due to the extremely low solubility of iron sulfide minerals, the Fe²⁺ released in reaction (2) is precipitated into solid FeS, as represented in reaction (4), instead of remaining in a dissolved state. The formation and transformation of iron sulfide minerals follow the Ostwald rippling rule.^[14] A brief discussion is provided below.

It is generally believed that mackinawite is the first phase formed in the Fe-S system and the precursor to the formation of other iron sulfide minerals.^[11, 12] Mackinawite is metastable and has the capacity to transform to other iron sulfide phases, such as pyrrhotite, depending on temperature and solution chemistry. Lennie et al. showed that the spontaneous transformation during exposure of dry mackinawite to X-rays and proposed that greigite forms by rearrangement of Fe cations within the cubic close-packed S array of mackinawite.^[15] Schoonen and Barnes determined the conversion rate of mackinawite to hexagonal pyrrhotite at 150-200°C and found that the conversion is accelerated with decreasing solution pH.^[16]

Pyrrhotite is also metastable with respect to iron disulfide pyrite. Qian et al. studied the transformation under hydrothermal conditions with temperature up to 220 °C at vapor-saturated pressures, and found that the reaction proceeded by a dissolution-reprecipitation mechanism under all conditions.^[17] Pyrite formation proceeded by direct replacement of pyrrhotite and, simultaneously, by overgrowth from solution. The overall reaction can be expressed as:



The above reactions are expressed in terms of sulfur addition.^[17] The transformation process can also be achieved by an iron loss mechanism:^[18]



A third pathway is similar to the first pathway but with H₂S is the oxidant:^[19]



Analysis results also showed different inorganic minerals on joint cut and flow coupling. This could be caused by flow dynamics. Flow coupling is a thick-walled tubular component installed in areas of high turbulence. Turbulence can affect precipitation reaction and also change the deposition and erosion of scale minerals on metal surface.^[20,21]

To prevent the formation of iron oxides on the outer side of joint cut and flow coupling, oxygen scavenger should be added in the packer fluid. To minimize the iron sulfide deposition on inner side, use of corrosion inhibitor is often the most cost effective mitigation method.

IV. CONCLUSION

XRD and XRF chemical composition analyses of corrosion samples in the form of metal cuttings require a special instrument configuration. In this study, a special XRD configuration and setup (x-ray point focus rather than line focus, and an open eulerian cradle) were adapted in order to handle these unconventional samples. XRD and XRF techniques have their advantages and disadvantages respectively. Therefore, the combined usage of XRD and XRF is absolutely necessary. Based on the analytical results, it can be concluded that the corrosion products of the tubular inner side were mainly iron sulfides whereas the corrosion products of the tubular outer side were mainly iron oxides, which indicated they were formed in different conditions.

ACKNOWLEDGEMENTS

The authors would like to acknowledge Saudi Aramco for the permission to publish this paper. Special thanks go to X-Ray Lab members for their help in the experiments.

REFERENCES

- [1] P.R. Roberge, Handbook of corrosion engineering, McGraw-Hill, New York, 2000, p. 7-8.
- [2] M.B. Kermani, L.M. Smith, CO₂ corrosion control in oil and gas production design consideration, The Institute of Materials, European Federation of Corrosion Publications, London, 1997, p. 3-4.
- [3] Champion Technologies, Corrosion mitigation for complex environments, Champion Technologies, Houston, 2012, p. 22-23.
- [4] D. Lusk, M. Gupta, K. Boinapally, Y. Cao, Armoured against corrosion, Hydrocarbon Engineering, 2008, 13, p. 115-118.
- [5] L.T. Popoola, A.S. Grema, G.K. Latinwo, B. Gutti, A.S. Balogun, Corrosion problems during oil and gas production and its mitigation, International Journal of Industrial Chemistry, 2013, 4, p. 1-15.
- [6] S. Shen, H. Sitepu, S.A. Hamoud, I.M. Taie, G. Alabedi, A.A. Sharani, B.F. Daajani, Use of XRD and XRF techniques to determine the chemical composition and crystallite size of metal matrix composite materials, Saudi Aramco Journal of Technology, 2010 winter issue, p. 50-55.
- [7] S. Shen, A.M. Sherik, H. Sitepu, S.R. Zaidi, S.A. Hamoud, Chemical composition determination of black powder samples by XRD and XRF, 13th Middle East Corrosion Conference & Exhibition proceedings, 2010, paper No 10096.
- [8] F. Shi, L. Zhang, J. Yang, M. Lu, J. Ding, H. Li, Polymorphous FeS corrosion products of pipeline steel under highly sour conditions, Corrosion Science, 2016, 102, p.103-113.
- [9] R.A. Berner, Sedimentary pyrite formation, American Journal of Science, 1970, 268, p. 1-23.
- [10] S.W. Poulton, M.D. Krom, J. Van Rijn, R. Raiswell, The use of hydrous iron (III) oxides for the removal of hydrogen sulphide in aqueous systems, Water Research, 2002, 36, p. 825-834.
- [11] S.N. Smith, M.W. Joosten, Corrosion of carbon steel by H₂S in CO₂ containing oilfield environments, CORROSION 2006, paper no. 06115 (Houston, TX: NACE, 2006).
- [12] A.G. Wikjord, T.E. Rummery, F.E. Doern, D.G. Owen, Corrosion and deposition during the exposure of carbon steel to hydrogen sulphide-water solutions, Corrosion Science, 1980, 20, 5, 6, p. 51-671.
- [13] S.N. Smith, B. Brown and W. Sun, Corrosion at higher H₂S concentrations and moderate temperatures, CORROSION 2011, paper no. 11081 (Houston, TX: NACE, 2011).
- [14] J.W. Morse, W.H. Casey, Ostwald processes and mineral paragenesis in sediments, American Journal of Science, 1988, 288, p. 537-560.
- [15] A.R. Lennie, S.A.T. Redfern, P.E. Champness, C.P. Stoddart, P.F. Schofield, D.J. Vaughan, Transformation of mackinawite to greigite: an in situ X-ray powder diffraction and transmission electron microscope study, American Mineralogist, 1997, 82, p. 302-309.
- [16] M.A.A. Schoonen and H.L. Barnes, Mechanisms of pyrite and marcasite formation from solution: III. Hydrothermal processes. Geochim. Cosmochim. Acta, 1991, 55, p. 3491-3504.
- [17] G. Qian, F. Xia, J. Brugger, W.M. Skinner, J. Bei, G. Chen and A. Pring, Replacement of pyrrhotite by pyrite and marcasite under hydrothermal conditions up to 220 °C: An experimental study of reaction textures and mechanisms, American Mineralogist, 2011, 96, p. 1878-1893.
- [18] R.T. Wilkin and H.L. Barnes, Pyrite formation by reactions of iron monosulfides with dissolved inorganic and organic sulfur species, Geochim. Cosmochim. Acta, 1996, 60, p. 4167-4179.
- [19] E. Drobner, H. Huber, G. Wachterhauser, D. Rose and K.O. Stetter, Pyrite formation linked with hydrogen evolution under anaerobic conditions, Nature, 1990, 346, p. 742-744.

- [20] L. Sutherland, C. Johnston and W. Taylor, The influence of turbulence (or hydrodynamic effects) on barium sulphate scale formation and inhibitor performance, 2013, SPE International Symposium on Oilfield Chemistry, paper no. 164070.
- [21] A. Quddus and L. Al-Hadhrami, Influence of solution hydrodynamics on the deposition of CaSO₄ scale on aluminum, Journal of Thermophysics and Heat Transfer, 2011, 25, p. 112-118.

The optimal configuration of turbines location in a wind farm using a Genetic Algorithm

DAOUDI Mohammed¹, ELKHOUZAI Elmostapha²

Laboratory of Engineering Didactic and Dynamic Systems University Hassan 1st Settat, Morocco

Abstract— The placement of wind turbines is a key technology for wind farm configuration, but the automatic placement of turbines is always still a difficult problem. The objective of every wind farm designer is producing as maximum as possible of energy, with minimal cost of installation. The improved wind and turbine models are formulated into an optimal control framework in terms of minimizing the cost per unit energy of the wind farm. In this study, a code Wind Farm Optimization using a Genetic Algorithm (WFOAG) is developed for optimizing the placement of wind turbines in wind farm to minimize the cost per unit power produced from the wind farm. A genetic algorithm is employed for the optimization. WFOAG is validated using the results from previous studies.

Keywords— wind farm; cost model, wake effect, optimization, wind turbine, genetic algorithm.

I. INTRODUCTION

Today, the part of production from renewable energy sources has increased dramatically compared to fossil fuels. This is generally due to some factors such as the high and rising price of traditional fossil fuels, during this, great social and environmental concerns and institutional support undertake to reduce foreign fossil fuels.

Many countries have already invested in green energy and they will invest even more because of dwindling resources of fossil fuels, the commitment of the Kyoto Protocol and the obligations for all countries with regard to the protection of the environment. By focusing on the types of renewable energy, it is a well known fact that wind energy has increased the most. That is why the development of an efficient tool for the design and construction of wind farms has a special importance. The design of the wind farm involves several factors. These range from maximum desired installed capacity for the wind farm, site constraints, noise assessment for noise sensitive dwellings, visual impact and the total cost. The fundamental aim, while designing a wind farm, is to maximize the power production while reducing the total costs associated with the wind farm. 'Micro-siting' is the process of optimizing the layout of the wind farm. This process is facilitated by the use of wind farm design tools (WFDTs) which are commercially available.

In this work, wind turbine placement in a wind farm is optimized using an objective function that represents the cost per unit power produced by the wind farm for a particular wind distribution function. The wind distribution function, in general, represents a model of wind variations in speed and direction averaged over a year, or many years. A genetic algorithm is employed for optimizing the placement of the wind turbines. An analytical wake model is utilized for modeling wind turbine wakes in the wind farm.

II. LITERATURE REVIEW

Several researchers have utilized analytical wake models to optimize the placement of wind turbines in a wind farm. Use of computational wake models has been rare owing to high computational costs involved in obtaining specific results for each wind condition under consideration. In order to achieve better results, some studies on wind turbines positioning were performed, where different optimization methods and wind farm models were used. The first work that implemented an optimization method for this problem was introduced by Mosetti et al. in 1994 [1], which adopted the genetic algorithm as an optimization tool. The study of Mosetti et al. was to develop an algorithm able to place wind turbines in a defined area where the goals of the optimization were maximizing the production and reducing the cost of implementation. Mosetti et al. opted for simple wind farm and cost modeling, because their focus was the effectiveness of the optimization process. In 2005, Grady et al. [2] attempted the same problem as Mosetti et al. They examined the same three cases as Mosetti. Authors have used the exact same approach as was by Mosetti et al. such as Jensen's analytical wake model and a genetic algorithm for optimization. Grady et al. showed that Mosetti et al.'s results are not optimum. They suggested that the probable cause is that the solution was not allowed to evolve for sufficient generations (i.e., it was not converged to the optimum point). Another work was developed by Marmidis et al. in 2008 [3], which used a different optimization method, the Monte Carlo method. Emami et al.[4] in 2010 proposes an improvement in wind farm layout optimization with the Jansens's wake model by

modification of the objective function, which takes into account the efficiency of wind turbines and the wind farm deployment cost.

TABLE 1
DETAILED DESCRIPTIONS OF PAST APPROACHES

Detailed Descriptions Past Approaches	Objective function	Cost/year	Technique used	Power	Efficiency
Mosetti et al.	Single objective	Same	Genetic algorithm	reported	Not considered a parameter
Grady et al.	Single objective	same	Genetic algorithm	reported	Not considered a parameter
Marmidis et al.	Single objective	same	Monte Carlo simulation	reported	Not considered a parameter
Emami et al.	Multi-objective	same	Genetic algorithm	reported	Considered and calculated in some cases

The literature review gives a clear vision that mostly research in the field of wind farm layout optimization focused only on the wind turbine positioning within the specific area of wind farm [5]. However the research on the wind farm area dimensions and fully utilization of upstream wind velocity is currently lacking in literature. The present work is based on the works mentioned above, as it also uses genetic algorithm as an optimization tool and a simple modeling of a wind farm. Nevertheless, new codifications have been adopted.

III. FORMULATION OF OPTIMIZATION PROBLEM

3.1 Probability density function

The wind speed histogram is approximated by a continuous function called the probability density function. This function expresses the probability (frequency or percentage of time) of occurrence of wind speed.

The probability density function is given by:

$$f(V) = \frac{k}{c} \left(\frac{V}{c}\right)^{k-1} \exp\left[-\left(\frac{V}{c}\right)^k\right] \quad (1)$$

The cumulative distribution function is given by:

$$F = \exp\left[-\left(\frac{V}{c}\right)^k\right] \quad (2)$$

The V value average and standard deviation σ of the distribution are expressed using the Γ function:

$$V = c \Gamma\left(\frac{1}{k} + 1\right) \quad (3)$$

$$\sigma = c \left| \Gamma\left(1 + \frac{2}{k}\right) - \Gamma^2\left(1 + \frac{1}{k}\right) \right| \quad (4)$$

Γ is an Eulerian function of the second kind defined by:

$$\Gamma(x) = \int_0^{\infty} t^{x-1} \exp(-t) dt \quad (5)$$

With $x \geq 0$; $t = \left(\frac{V}{c}\right)^k$; $(x - 1) = \left(\frac{1}{k}\right)$

The integration of $f(v)$ between V and ∞ give the expression of the distribution function $f(v)$. To represent the distribution of the wind frequency using the Weibull distribution, there is a probability density function:

$$f(v) = \left(\frac{k}{c}\right) \left(\frac{v}{c}\right)^{k-1} \exp\left(-\left(\frac{v}{c}\right)^k\right) \quad (6)$$

Where $f(v)$ is the probability density at the speed V (m/s), K is the shape of the curve factor (dimensionless), C is the scale of the curve factor in m/s.

3.2 Wake model

Turbines interact with the wind captures part of the kinetic energy and are converted to usable energy. According to the first law of thermodynamics, this energy extraction creates a gap between the outgoing wind turbine and the oncoming wind turbine. Thus, the wind speeds at the rear of the turbine is lower than the wind speed upstream and consequently a reduction in output power is generated by the turbines. The wake effect also causes high levels for turbulence in the wind turbines, giving rise to an additional mechanical strain, which may reduce their lifetime.

Many studies on the wake effect were conducted, and several models have been developed by researchers, as mosaic tile model [6], the Frandsen model [7], Ainslie [6] model, the model Jensen [9] and CFD (Computational Fluid Dynamics) model [10]. The choice of model depends on the desired accuracy of the prediction and the calculation time. A wake models most widely used, developed by Jensen [9], was chosen for this study because it provides sufficient accuracy and a reduction in computation time. The turbine interact with the wind, capture a portion of its kinetic energy and converts it into useable energy, this extraction of energy creates a gap between the outgoing wind turbine and the oncoming wind turbine. Thus, the wind speeds at the rear of the turbine is lower than the downstream speed of the wind, as a result it decreases the production of output energy [11]. The wake effect also causes high levels of turbulence in the outgoing wind turbines, giving rise to an additional mechanical stress, which may affect them, this behavior caused by the turbulent is neglected in this study because it does not affect directly output power. In both works of Mosetti and Grady's [1-2] the model used is similar to the model developed by Jensen [9] in 1986. Here we assume that the movement is kept inside the wake.

For a single turbine, the downstream wake zone will be considered as a trapezoid such that the average speed of the wind can be expressed by the following equation:

$$u = u_0 \left[1 - \frac{2a}{\left(1 + \alpha \left(\frac{x}{r}\right)^2\right)^2} \right] \tag{7}$$

Where α is the entrainment Constant, a is the axial induction factor, x is the distance from the turbine, and r is the radius of the turbine downstream, as shown in Figure 1.

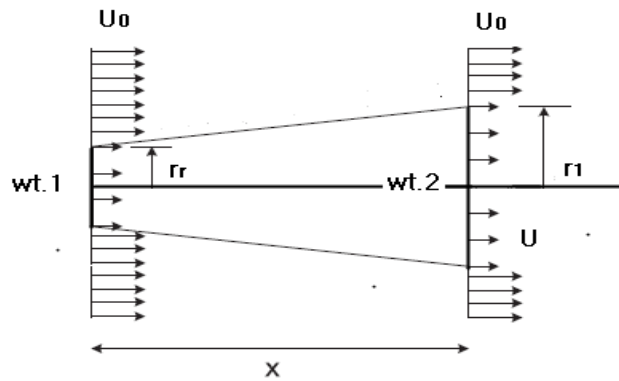


FIGURE 1. Single Wake

The relationships between r , r_r the radius of turbine and C_T the thrust coefficient are represented in the equations:

$$r = r_r \sqrt{\frac{1-a}{1-2a}} \tag{8}$$

$$C_T = 4a(1 - a) \tag{9}$$

The entrainment Constant is empirically given by:

$$\alpha = \frac{0.5}{\ln\left(\frac{z}{z_0}\right)} \tag{10}$$

Where z is the hub height of the wind turbine, and z_0 is the surface roughness of the site. When the turbine downstream is not completely immersed in a wake, if A_w is the part of the rotor area that is inside the upstream turbine wake, as shown in Figure. 2, the effect of the corresponding deficit must be reduced according to:

$$(U_p - U_0)^2 = \frac{4A_w}{\pi D_0^2} (U - U_0)^2 \tag{11}$$

Assuming that R and r are respectively the radii of the bigger and lower circumferences (general but not necessarily the wake and rotor ones respectively) and X is the distance between their centres, the overlapped area A_w yields:

$$A_w = R^2 \cos^{-1} \left(\frac{R^2 + X^2 - r^2}{2RX} \right) - R^2 0.5 \sin \left(2 \cos^{-1} \left(\frac{R^2 + X^2 - r^2}{2RX} \right) \right) + r^2 \cos^{-1} \left(\frac{R^2 - X^2 - r^2}{2RX} \right) - r^2 0.5 \sin \left(2 \cos^{-1} \left(\frac{R^2 - X^2 - r^2}{2RX} \right) \right) \tag{12}$$

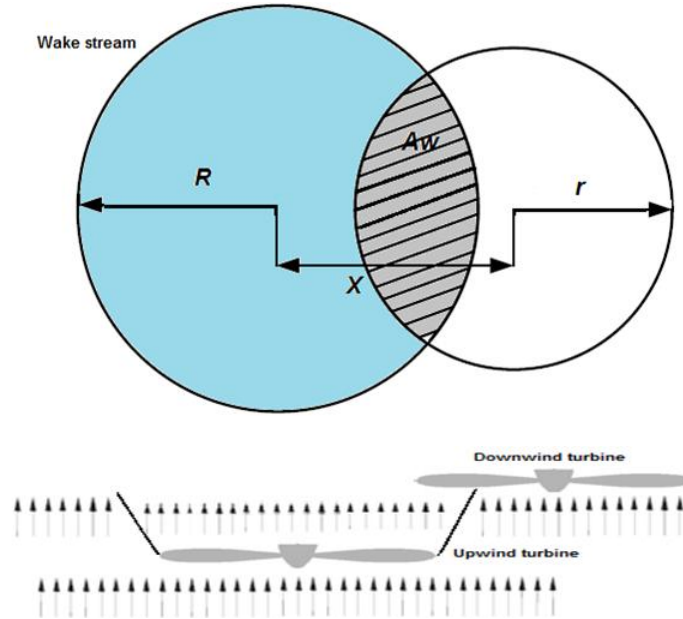


FIGURE 2. The Shade Area of A Downstream Wind Turbine in Partial Wakes.

For multiple wakes we supposed that the loss of kinetic energy is equal to the sum of the energy losses. So, for N turbines, the downstream speed can be expressed by the following expression:

$$u_i = u_0 \left[1 - \sqrt{\sum_{i=1}^N \left(1 - \frac{u}{u_0} \right)^2} \right] \tag{13}$$

3.3 Cost model

The electricity generated by an aero generator, is a function of the local wind speed. Furthermore, the hub height, the thrust coefficient and the rotor diameter also affects the extracted power.

The total power P extracted from the wind is a function of the local section and wind speed, as shown in the following expression:

$$P = \sum_{i=0}^N 0.3u_i^3 \tag{14}$$

To calculate the total cost, we modelled the investment cost such a way that only the number of wind turbines must be taken into consideration.

The total cost per year for the entire wind farm can be expressed as follows:

$$\text{cost} = N \left(\frac{2}{3} + \frac{1}{3} e^{-0.00174N^2} \right) \tag{15}$$

Where N is the total number of wind turbines.

The objective function that will lead to optimization (minimum cost per unit of energy produced) is expressed as follows:

$$\text{objective function} = \frac{\text{cost}}{P_{\text{total}}} \tag{16}$$

Where P_{total} is the total production, while the cost is calculated as mentioned in equation (15).

Minimize the objective function leads to a solution with the lowest cost of producing wind energy [12].

Wind turbines must be spread over the site to share the best wind between many machines.

3.4 Efficiency Model

Efficiency is determined as a ratio between the amount of energy extracted from the wind farm and the total energy without wake. The numerator represents the actual energy extracted from the rotor of each wind turbine, considering the Betz limit of aerodynamic theory. The wind farm efficiency can be formulated using the equation depending on the number of wind turbines.

Total power produced in wind farm when considering wake effect can be calculated by using equation:

$$P_{\text{Total}} = \sum_{i=0}^{N_T} (0.3u_i^3) \quad (17)$$

Equation (15) is used to calculate the wind farm total power without wake effect:

$$P_{\text{WT}} = P \times N_T = N_T(0.3u_i^3) \quad (18)$$

Where, P , is the rated capacity of each wind turbine.

The overall efficiency of the wind farm is calculated by using equation (19), as follows:

$$\text{Efficiency} = \frac{P_{\text{Total}}}{P_{\text{WT}}} = \frac{\sum_{i=0}^{N_T} (0.3u_i^3)}{N_T(0.3u_i^3)} \quad (19)$$

IV. APPLICATION OF GENETIC ALGORITHMS

In this study, we follow [1, 2, 3, 4] study the turbine placement problem on a flat and square farm. The wind farm is divided into 10×10 cells, the width of which is set to be five times that of turbine rotor diameter for safe operations. The center of each cell is the possible position of the turbines. The objective of the optimization is to determine the cells to place turbines so as to minimize the cost per unit energy produced.

The wind turbines placement problem is of discrete type and presents an infinity of optimal solutions, which somehow discards the applicability of optimization methods based on local gradients [1]. Assuming a wind farm described by a 10×10 matrix, where each element may contain or not a wind turbine, you can find 2^{100} different configurations, making it impractical to use conventional computers for such problem's analysis.

According to Mosetti et al., for this case, the genetic algorithm is a good tool in the search of the best configuration. This method is able to find an optimal solution to problems of great complexity, eliminating the need of evaluating each individual solution [1].

The optimization algorithms are divided into two main groups: deterministic (based on differential calculus) and random (probabilistic). The deterministic methods are based on the calculation of derivatives or approximations thereof, seeking information from the gradient vector to find the point in which it is annulled, or to find its direction [13].

The random methods use the results of the objective function, which can be difficult to represent, discontinuous, non-differentiable, multimodal (with several minimum and maximum points). These methods look for the optimal value through operating rules of probability in a "randomly oriented" way [13]. One of the main random methods is the genetic algorithm.

Genetic algorithms are probabilistic search algorithms, which are based on the logic of natural selection and the survival of the fittest to commit certain remarkable tasks. Unlike calculus-based methods, genetic algorithms are robust, global, and do not require the existence of derivatives [14].

Since the optimal micro-sitting problem is quite complicated and involves many independent variables, it cannot be solved by traditional gradient-based optimization methods. A genetic algorithm is employed to solve such a problem. In the genetic algorithm, the selection, crossover and mutation are the fundamental operators [14]. The selection operation chooses two parents from the population for crossing. The crossover operator takes two parent solutions to produce a child. The crossover probability P_c is usually between $0.6 \sim 0.9$. The mutation operator introduces new genetic structures into the population by randomly modifying some of its building blocks. It avoids the trap of local minima and maintains diversity in the population. The mutation probability P_m is generally between $0.01 \sim 0.1$. In the genetic algorithm, a few of the best chromosomes should be copied to the new population in case that such individuals can be lost by crossover or mutation operators [14].

After the occurrence of crossover the mutation operator is applied. This operator inverts the values of some genes i.e., a 0 gene can turn to 1 or a 1 gene can turn to 0. This operator is used for increasing the diversity of the chromosomes in a population. Figure 3, adapted from [2], illustrate crossover and mutation operators.

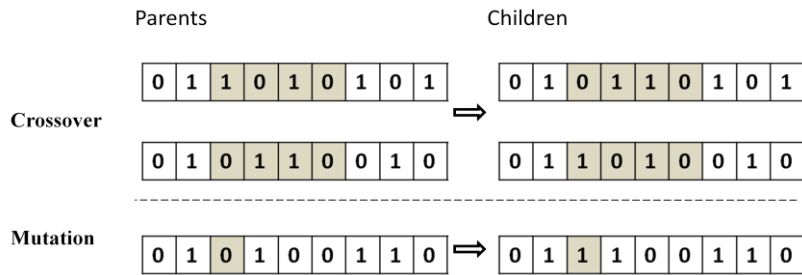


FIGURE 3. Crossover and Mutation Operators

In the present study, the field is described by a code matrix composed of m by n "zeros" and "ones", where 0 simply means a space without the presence turbine 1 and a wind turbine, as shown in figure 4.

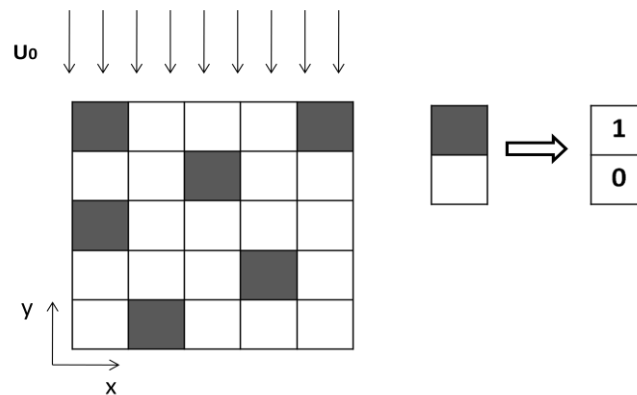


FIGURE 4. Codification Method

V. NUMERICAL PROCEDURE

The code is attached to the WFOAG optimization tool by genetic algorithm. The flowchart in figure 5 explains the process through which WFOAG is used as the objective function, generating the necessary results to evaluate individuals created. Basically, the optimization process is divided in three stages: Pre-processing (Initialization), Processing (genetic algorithm) and Post processing (a result evaluation).

5.1 Pre-processing

In the first stage, are specified the optimization parameters as: Number of input variables: for the proposed problem, the only variable input is the matrix position (layout of the wind farm); Size of initial population: the total number of solutions that are generated randomly for the first generation; Restrictions: In order to avoid unfeasible evaluations of individuals, as restrictions are imposed minimum production or efficiency; Optimization criteria: the optimization criteria include the maximum number of iterations (called generations), the probability of crossover, mutation and selection, and optimization method.

5.2 Processing

After the initialization process, starting from a given initial population, the fitting of each individual is evaluated by the objective function (WFOAG), and by the best individuals, the next generation will be designed. This new population is obtained through crossover and mutation among individuals with higher fitting in random regions.

In the next step optimization criteria are checked if they are satisfied or not. When the optimization criteria are not met, all the solutions are ranked based on their objective function values. A solution with small objective function value is better as its cost per unit power is smaller and is placed before other solutions with larger objective function value. For example, a solution with objective function value of 0.02 is placed before a solution with objective function value of 0.03.

After ranking is completed, some solutions are selected based on which new solutions are created (reproduced). This selection of solutions is affected by the ranking done in previous step and a solution with good ranking has a better chance of

being selected. New solutions are created but some solutions are copied from original set of solutions to the new set of solutions. These selected few solutions are one of the best in terms of the ranking and are called elite count.

The next step before new set of solutions (new population) is ready is called Mutation. In this step some random changes are made in few solutions. This step is very important as it helps in maintaining diversity in the solution set. This new solution set is analyzed by WFOAG and this iterative procedure continues until one of the optimization criteria is satisfied. In the simulation, the type of selection is set as (Stochastic uniform), the type of crossover is set as (scattered) with the crossover probability $P_c = 0.8$, and the type of mutation set as (Uniform) with the mutation probability $P_m = 0.05$.

5.3 Post-processing

Just the once computations have stopped, the results are exported from the WFOAG and the exported structure is saved to a file for later use. The coordinates of all the wind turbines are saved in a separate variable and analyzed to determine the power produced. The layout can be plotted as per the requirement.

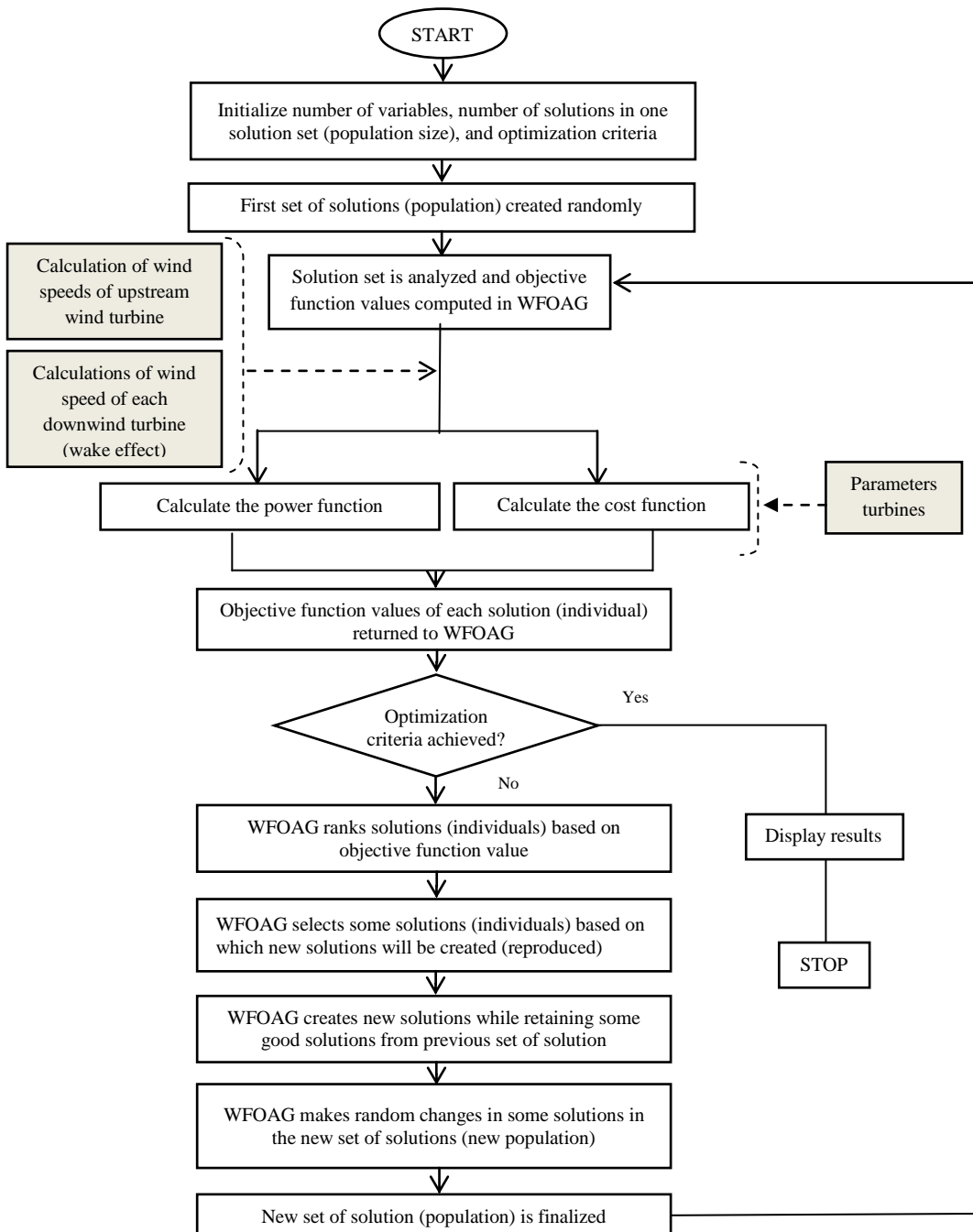


FIGURE 5. Flowchart Describing the Optimization Process

VI. RESULTS AND DISCUSSIONS

6.1 Influence of wake effect on wind speeds of each wind turbine

In order to analyze how wind speeds of each turbine are affected by wakes, two different scenarios have been simulated. The first, a wind farm composed of 16 wind turbines (4X4) is presented. The y-axis is fixed to 0° which it is assumed to be coincident with the prevailing wind direction. The wind farm layout, as well as the wake effect caused by a particular incoming wind direction of 30°, is shown in Fig. 6(a). The distance between two nearby wind turbines in axis y (Dist_y) is 7 rotor diameters (D) and 5 rotor diameters (D) in axis x (Dist_x).

In Fig. 6 (b), the wind speed of each wind turbine is shown. As expected, the wind speeds obtained by means of simulation are consistent with the above mentioned. The average wind speed for the entire wind farm is 8 m/s, which is relatively high, although lower than full load, and therefore the thrust coefficient has not dropped significantly as at high wind speeds.

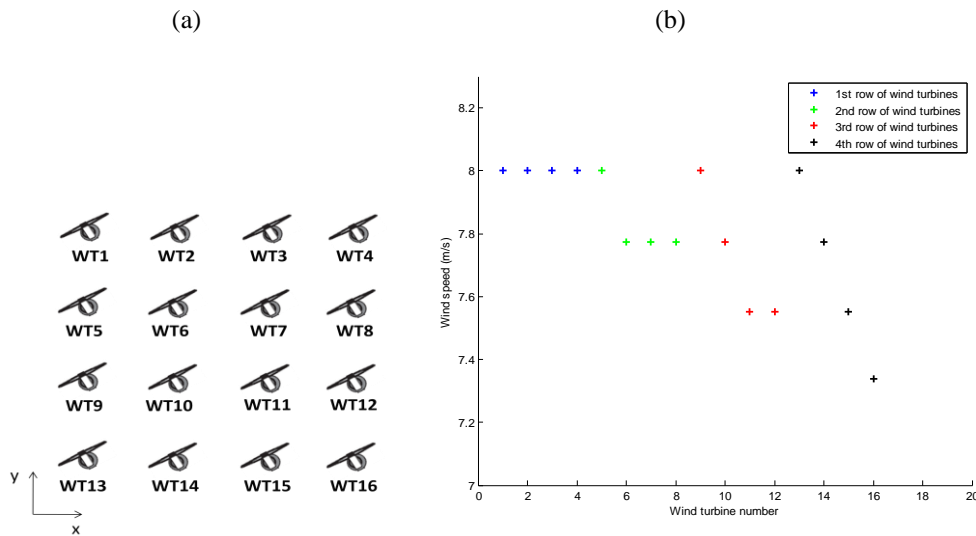


FIGURE 6. (a) Wake Decay for A 16 Wind Turbine Array (4x4) Spaced 7d (Dist_Y) And 5d (Dist_X) When The Prevailing Wind Direction Is 30°. (b) Wind Speeds of Each Turbine.

The second wind farm scenario consists of 16 wind turbines laid, out in 4 rows with a spacing of about 5 rotor diameters (D) between and along rows (Dist_x and Dist_y). The incoming wind direction is coincident with the prevailing wind direction, that is, 0° (see Fig. 7(a)).

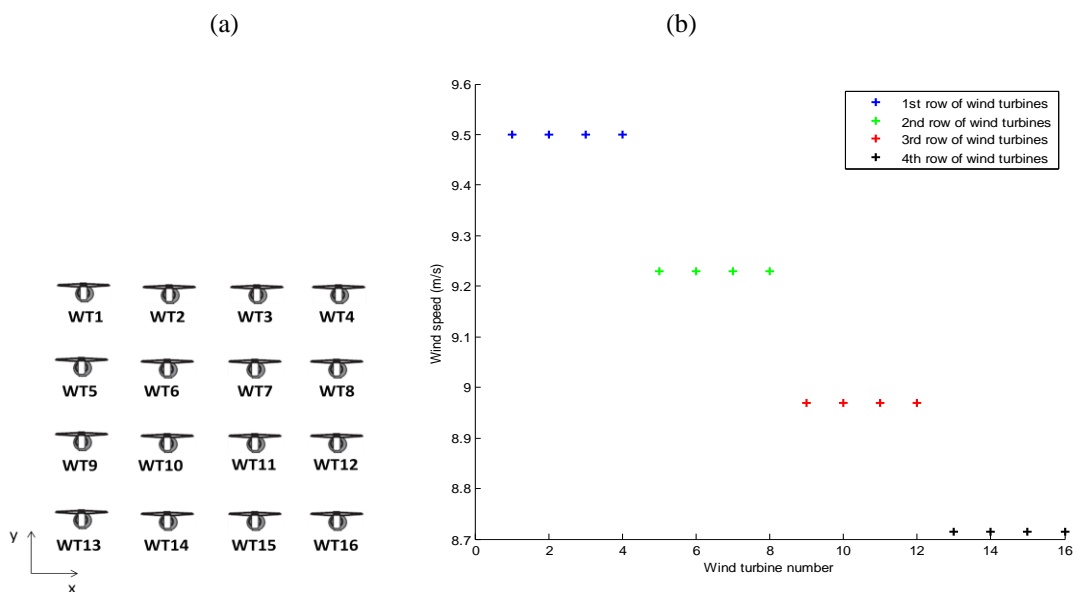


FIGURE 7. (a) Wake Decay For A 16 Wind Turbine Array (4x4) Spaced 5d (Dist_Y) And 5d (Dist_X) When The Prevailing Incoming Wind Direction Is 0°. (b) Wind Speeds of Each Turbine.

In this case, the rows 2, 3 and 4 are affected by wakes. The wind turbines located in the second row (green WTs) are affected by a single wake, whereas, the turbines in the third and fourth row are affected by multiple wakes.

For both scenarios (30° and 0°), the entrainment constant k is 0.04. As in the previous case, the wind speeds of each wind turbine are depicted in Fig. 7(b) and are consistent with the wind farm layout of Fig. 7(a). The average wind speed for the entire wind farm is 9.5 m/s.

6.2 Comparison to previously published wind farm optimization cases

In a way to verify the WFOAG performance, some simulations were done and the results were compared with other authors' works [1, 2, 3, 4]. These works were chosen because they use the same parameters used by Mosetti et al. model as well as Jensen's wake model [9] and probabilistic algorithms as optimization tool, guaranteeing control and reliability of results.

Without loss of generality, we suppose the wind speed distribution in both cases satisfies the Weibull function. The shape parameter of the Weibull function is set to $k = 2$, which represents a typical wind condition for turbine operations.

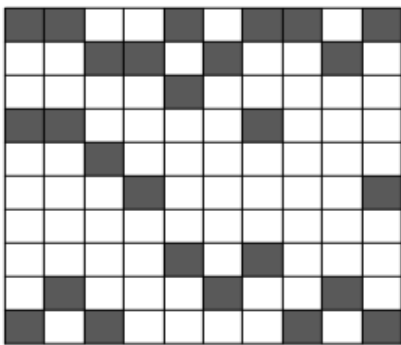
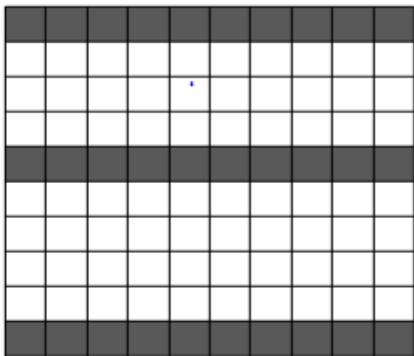
The scale parameter of the function is calculated as $c = 13.54$. The surface roughness of the wind farm is $z_0 = 0.3m$. The parameters of the wind turbine are shown in Table 2.

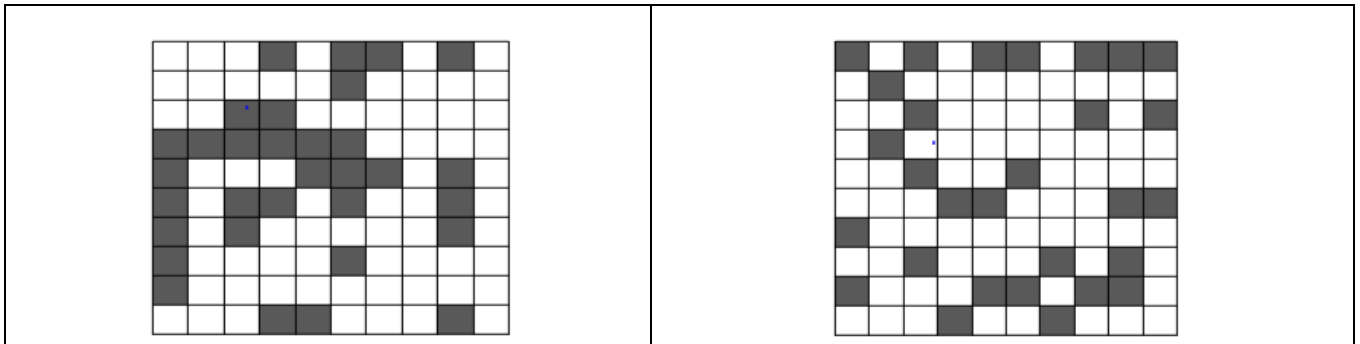
TABLE 2
CARACTÉRISTIQUES OF TURBINES

Description	Parameter	value
Hub height	z	60 m
Radius of the rotor	r_r	40 m
Thrust coefficient	C_t	0.88

In order to estimate the optimal number of wind turbines and for comparative purposes we will take the following basic conditions: uniform wind direction and speed steady wind of 12 m / s.

TABLE 3
WFOAG RESULTS FOR COMPARISON WITH PREVIOUS STUDIES

Mosetti et al. Number of turbines 26 Total power 12921 KW/ year objective function 0.0016197 Efficiency 95.5%	Grady et al. Number of turbines 30 Total power 14764KW/ year objective function 0.0015436 Efficiency 94.6%	Emami Number of turbines 26 Total power 12921KW/ year objective function - Efficiency 95.5%
		
Marmidis Number of turbines 32 Total power 13467 KW/ year objective function - Efficiency 80.9%	Present results Number of turbines 29 Total power 14664 KW/ year objective function 0.0014710 Efficiency 95.4%	



This case has been discussed in detail in [1, 2, 3] where different approaches were used. Choosing this case study was performed for comparison. In this case, turbines affect each other. This makes it difficult to place the turbines through the experience. To describe the placement of a wind farm, it is necessary to evaluate parameters: layout Efficiency (%) and electricity production (kWh). To calculate this parameter a code has been developed which considers the wake effect as the main influence on the decline in production of a wind farm. This code will be used as the objective function of the optimization algorithm, and will provide the necessary parameters for comparison and selection of the best layouts.

The input parameters are the velocity of the not disturbed flow upwind turbine, the rotor diameter of wind turbines, the hub height, the terrain roughness and the power curve with values of the thrust coefficient and power turbine velocity for any wind within the operating range. This code considers possible interactions between wakes. A wind turbine can be influenced by more than one wake from upwind turbines, plus there is the possibility of overlap between wakes.

Some simplifying assumptions were considered in the code developing. They are: all the turbines in the wind farm are equal, i.e. have the same height of the cube, the same rotor diameter, same number of blades and the same power curve, the ground location of the wind farm is perfectly flat, uniform roughness, the turbines are arranged in a matrix, a result for a single value of velocity and direction.

The layouts proposed by these authors were simulated in WFOAG to obtain the results for comparison, making it as impartial as possible. Then a different wind farm configuration was inserted in the WFOAG (under the same conditions used by Mosetti et al.) to be optimized. The aim of this process was to verify the capacity of the WFOAG to achieve a layout performance near or higher than the proposed by the authors. The simulated layouts are illustrated in Table 3.

VII. CONCLUSION

The placement of wind turbines is an initial step in the wind farm design and forms the foundation for the efficient operation of the farm. At present, empirical schemes are commonly adopted. As the wind condition becomes complicated, systematic approaches such as genetic algorithms are needed to reach an optimal or suboptimal design. This paper further previous research on genetic algorithm placement by incorporating more appropriate models of wind speed distributions and turbine power curves. Simulation results indicate that the new genetic-algorithm scheme can improve wind farm performance, which expands more computation due to complicated models. It is of importance to study more realistic situations, for example, to use a more relevant wind turbines probably with pitch control systems, to use a cost model including cabling, to study relatively complex terrain layouts.

REFERENCES

- [1] Mosetti G, Poloni C, Diviacco B. Optimization of wind turbine positioning in large wind farms by means of a genetic algorithm. *Journal of Wind Engineering and Industrial Aerodynamics*. 1994; 51(1):105-16.
- [2] Grady SA, Hussaini MY, Abdullah MM. Placement of wind turbines using genetic algorithms. *Renewable Energy*. 2005; 30(2):259-70.
- [3] Marmidis G, Lazarou S, Pyrgioti E. Optimal placement of wind turbines in a wind park using Monte Carlo simulation. *Renewable Energy*. 2008; 33(7):1455-60.
- [4] Emami A, Noghreh P. New approach on optimization in placement of wind turbines within wind farm by genetic algorithms. *Renewable Energy*. 2010; 35(7):1559-64.
- [5] Shakoor R, Hassan M Y, Raheem A, Rasheed N, Mohd Nasir MN, editors. Wind farm layout optimization by using definite point selection and genetic algorithm. 2014 IEEE International Conference on Power and Energy (PECon 2014); 2014; IEEE Digital Explore.

-
- [6] Rathmann O, Frandsen S, Barthelmie R. Wake modelling for intermediate and large wind farms. In: Wind energy conference and exhibition; 2007.
- [7] Frandsen S, Barthelmie R, Pryor S, Rathmann O, Larsen S, Højstrup J, et al. Analytical modelling of wind speed deficit in large offshore wind farms. *Wind Energy*; 2006.
- [8] Ainslie JF. Calculating the flowfield in the wake of wind turbines. *Journal of Wind Engineering and Industrial Aerodynamics* 1988;27:213e24.
- [9] Jensen NO. A note on wind generator interaction; 1983. Technical Report RISØ-M-2411, Denmark.
- [10] Rthor P-E, Bechmann A, Sørensen NN, Frandsen ST, Mann J, Jørgensen HE, et al. A CFD model of the wake of an offshore wind farm: using a prescribed wake inflow. *Journal of Physics: Conference Series* 2007; 75: 012047.
- [11] Chompoo-inwai C, Leelajindakraierk M, Banjongjit S, Fuang foo P, Lee W-J. Design optimization of wind power planning for a country with low-medium wind-speed profile. *IEEE Transactions on Industry Applications* 2008; 44(5):1341-7.
- [12] R. Dechter and I. Meiri. Experimental evaluation of preprocessing techniques in constraint satisfaction problems. In *Proc. of the 11th IJCAI*, pages 271-277, Detroit, MI, 1989.
- [13] S. F. Saramago, G. T. S. Oliveira, *Estratégias de Evolução Diferencial Aplicadas a Problemas de Otimização Restritos*, 15° POSMEC – Simpósio do Programa de Pós-Graduação em Engenharia Mecânica – UFU, 2005.
- [14] S.N. Sivanandam and S.N. Deepa, *Introduction to Genetic Algorithms*, New York:Springer, 2008.

Improvement of Biometric Authentication System Applying Fingerprint

Fatamatuz Ayasa Khan

Computer Science & Engineering, Islamic University, kushtia, Bangladesh

Abstract—The biometric system plays an important role in everyone life. To identify one identity, the finger is one of many forms of the biometrics are generally used. The fingerprint is the verified function to identify a match between two person's fingerprints. Here a simple and effective system for biometric fingerprint based voter identity system has been proposed that is based on image enhancement and correct minutiae extraction. Automatic and reliable extraction of minutiae from fingerprint images is a critical step in fingerprint matching. In this research a fast fingerprint enhancement and minutiae extraction algorithm have been presented which improve the clarity of the ridge and valley structures of the input fingerprint images based on the frequency and orientation of the local ridges and thereby extracting correct minutiae.

Keywords— *Biometric System, Identify Fingerprint, Authentication System, Person Identification.*

I. INTRODUCTION

A biometric system gives automatic recognition of an individual based on some sort of unique feature or characteristic possessed by the individual. Biometric systems have been created based on fingerprints, facial features, voice, hand geometry, handwriting, the retina [1], and the systems work by first capturing a sample of the feature, such as recording a digital sound of mathematical function into a biometric template. The biometric template will provide a normalized, efficient and highly discriminating representation of the feature, which can then be objectively compared with other templates in order to determine identity. Most biometric systems allow two modes of operation. An enrolment mode for adding templates to a database, and an identification mode, where a template is created for an individual and then a match is searched for in the database of pre-enrolled templates.

A fingerprint is the pattern of curved lines on the end of a finger or thumb that is distinctive in every person or a mark left by this pattern. However, shown by intensive research on fingerprint recognition, fingerprints are not distinguished by their ridges and furrows, but by Minutia, which are some abnormal points on the ridges.

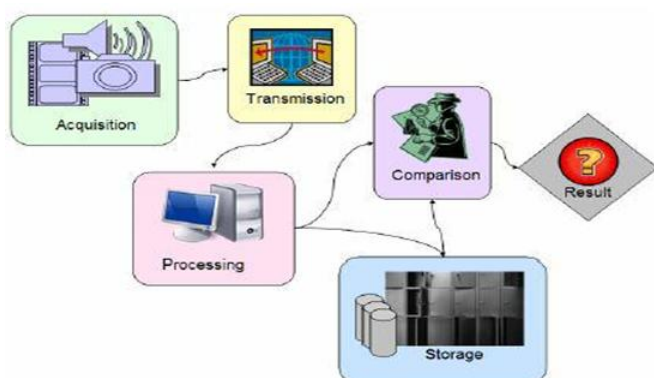


FIGURE 1: Characteristic of biometric system

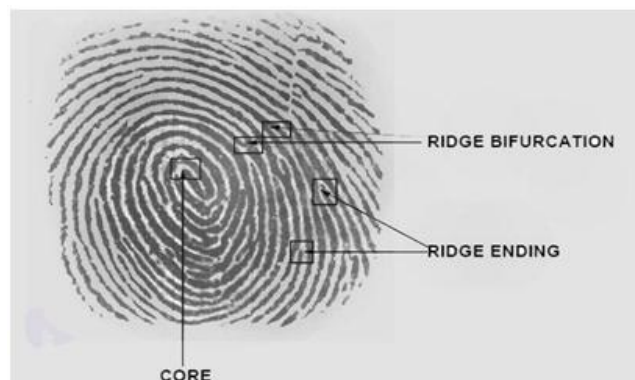


FIGURE 2: Minutia (Ending is also called Termination and Bifurcation is also called Branch)

Fingerprint-based person identity system can progress the user identification process by utilizing biometric recognition. Fingerprints are unique to each person and different finger impressions of the same user look different. Minutiae Based Matching is a system in which minutiae are extracted from a fingerprint and stored as sets of points in a two-dimensional plane and then minutiae of the fingerprint to be recognized are extracted and matched with the stored points. Minutiae matching essentially consist of finding the alignment between the template and the input minutiae sets that result in the maximum number of minutiae pairings. Generally, elements of this system are the sensor, minutia extractor, minutia matcher and a database.

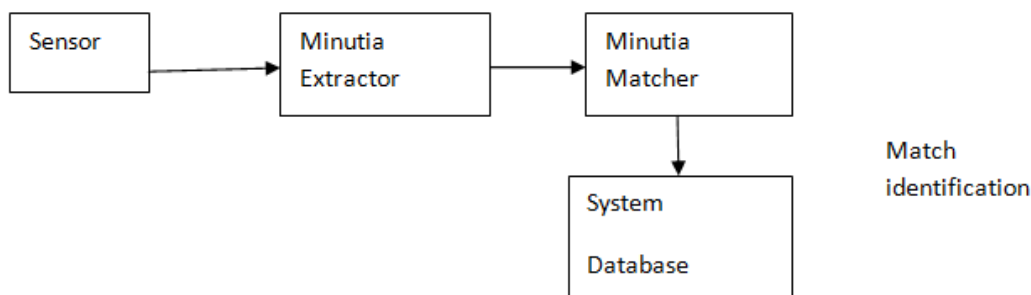


FIGURE 3: Block diagram of person identity system using fingerprint

Personal identification is to associate a specific individual with an identity. It plays a major role in our society, in which questions related to the identity of an individual such as “Is this the person who he or she claims to be?”, “Has this applicant been here before?”, “Should this individual be given access to our system?” “Does this employee have the authorization to perform this transaction?” etc are asked millions of times every day by hundreds of thousands of organizations in financial services, health care, electronic commerce, telecommunication, government, etc. With the rapid growth of information technology, people are becoming even more and more electronically connected. As a result, the capacity to achieve highly accurate automatic personal identification is becoming more critical. Traditionally, passwords (knowledge-based security) and ID cards (token-based security) have been used to restrict access to systems.

In the world of computer security, biometrics refers to authentication techniques that rely on measurable physiological and different characteristics that can be automatically verified. In other words, we all have unique personal attributes that can be utilized for distinctive identification purposes, including a fingerprint, the pattern of a retina, and voice characteristics. Strong or two-factor authentication—identifying oneself by two of the three methods of something you know (for example, a password), have (for example, a swipe card), or is (for example, a fingerprint)—is becoming more of a genuine standard in secure computing environments. Some personal computers today can include a fingerprint scanner where you place your index finger to provide verification. The computer analyzes your fingerprint to determine who you are and, based on your identity followed by a pass code or pass phrase, allows you different levels of access. Access levels can include the ability to open sensitive files, to use credit card information to make electronic purchases, and so on.

II. SYSTEM DESIGN

A fingerprint recognition system constitutes of fingerprint acquiring devices, minutia extractor, and minutia matcher. For fingerprint acquisition, optical or semi-conduct sensors are widely used. They have high efficiency and acceptable accuracy except for some cases that the user’s finger is too dirty or dry.

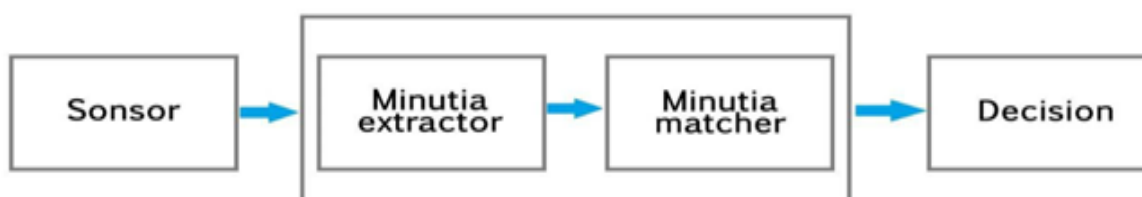


FIGURE 4: Block diagram of Simplified Fingerprint Recognition System

III. ALGORITHM

To implement a minutia extractor, a three-stage approach is widely used by researchers. They are preprocessing, minutia extraction and post-processing stage. For the fingerprint image preprocessing stage, Histogram Equalization and Fourier Transform are used to do image enhancement and then the fingerprint image is binarized using the locally adaptive threshold method. The image segmentation task is fulfilled by a three-step approach: block direction estimation, segmentation by direction intensity and Region of Interest extraction by Morphological operations.

For minutia extraction stage, the iterative parallel thinning algorithm is used. The minutia marking is a relatively simple task. For the post-processing stage, a more rigorous algorithm is developed to remove false minutia. The minutia matcher chooses any two minutiae as a reference minutia pair and then matches their associated ridges first. If the ridges match well, the two fingerprint images are aligned and matching is conducted for all the remaining minutiae.

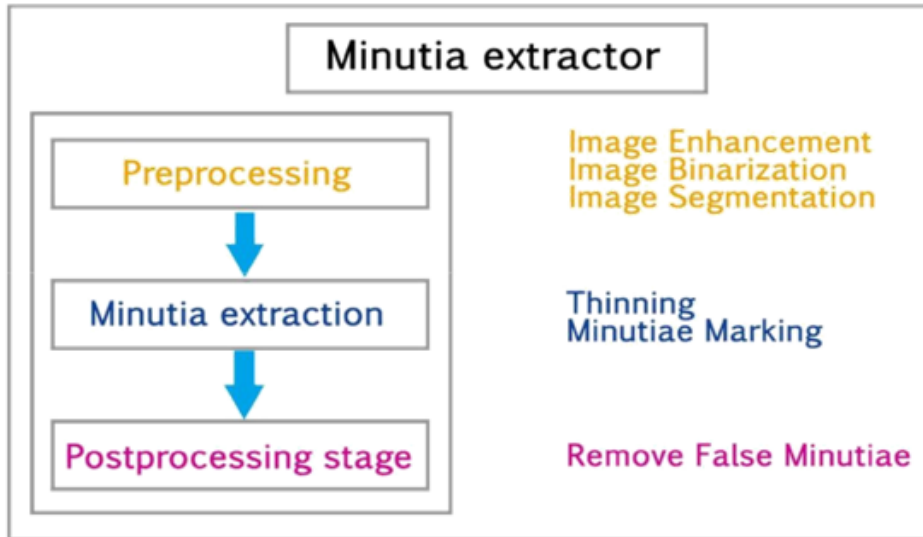


FIGURE 5: Block Diagram of minutia extractor of Fingerprint Recognition system

IV. FINGERPRINT IMAGE PRE-PROCESSING

Fingerprint Image Enhancement: Two Methods are adopted in my fingerprint recognition system; a. Histogram Equalization b. Fourier Transform.

a. The right side of the following figure [Figure 6] is the output after the histogram equalization.



FIGURE 6: Histogram Enhancement Original Image (Left). Enhanced image (Right)

b. Divided the image into small processing blocks (32 by 32 pixels) and perform the Fourier transform according to $F(u, v)$, where $F^{-1}(F(u, v))$ is done by:

$$F(u, v) = \sum_{r=0}^{M-1} \sum_{y=0}^{N-1} f(x, y) * \exp\{j2\pi * (\frac{ux}{M} + \frac{vy}{N})\}$$

For $u = 0, 1, 2, \dots, 31$ and $v = 0, 1, 2, \dots, 31$.

In order to enhance a specific block by its dominant frequencies, multiply the FFT of the block by its magnitude a set of times. Where the magnitude of the original FFT = $abs(F(u, v)) = |F(u, v)|$.

Get the enhanced block according to

$$g(x, y) = F^{-1}\{F(u, v) \times |F(u, v)|^k\}$$

Where $F^{-1}(F(u, v))$ is done by,

$$f(x, y) = \frac{1}{MN} \sum_{r=0}^{M-1} \sum_{y=0}^{N-1} f(x, y) * \exp\{j2\pi * (\frac{ux}{M} + \frac{vy}{N})\}$$

for $x = 0, 1, 2, \dots, 31$ and $y = 0, 1, 2, \dots, 31$.

While having a higher "k" improves the appearance of the ridges, filling up small holes in ridges, having too high a "k" can result in false joining of ridges. Thus a termination might become a bifurcation. Figure 7 presents the image after FFT enhancement.



FIGURE 7: Fingerprint Enhancement by FFT Enhanced image (right) Original image (left)

The enhanced image after FFT has the improvements to connect some falsely broken points on ridges and to remove some spurious connections between ridges. The shown image at the left side of figure 7 is also processed with histogram equalization after the FFT transform. The side effect of each block is obvious but it has no harm to the further operations because I find the image after consecutive binarization operation is pretty good as long as the side effect is not too severe.

Fingerprint Image Binarization: Fingerprint Image binarization is to transform the 8-bit Gray fingerprint image to a 1-bit image with 0-value for ridges and 1-value for furrows. After the operation, ridges in the fingerprint are highlighted with black color while furrows are white. A locally adaptive binarization method is performed to binarize the fingerprint image. Such a named method comes from the mechanism of transforming a pixel value to 1 if the value is larger than the mean intensity value of the current block (16x16) to which the pixel belongs in Figure 8.



FIGURE 8: Fingerprint image after adaptive binarization, Binarized image (right), original image (left)

Fingerprint Image Segmentation: Generally, only a Region of Interest (ROI) is useful to be recognized for each fingerprint image. The image area without effective ridges and furrows is first discarded since it only holds background information. Then the bound of the remaining effective area is sketched out since the minutia in the bound region is confusing with that spurious minutia that is generated when the ridges are out of the sensor.

To extract the ROI, a two-step method is used. The first step is blocked direction estimation and direction variety check, while the second is intrigued by some Morphological methods.

- a) **Block direction estimation:** Estimate the block direction for each block of the fingerprint image with $W_x W_y$ in size (W is 16 pixels by default). The algorithm is:
1. Calculate the gradient values along x-direction (g_x) and y-direction (g_y) for each pixel of the block. Two Sobel filters are used to fulfill the task.
 2. For each block, use following formula to get the Least Square approximation of the block direction.

$$tg2\beta = 2(g_x * g_y) / (g_x^2 - g_y^2) \text{ for all the pixels in each block}$$

The formula is easy to understand by regarding gradient values along x-direction and y-direction as cosine value and sine value. So the tangent value of the block direction is estimated nearly the same as the way illustrated by the following formula.

$$tg2 = 2sin\ cos / (cos^2 - sin^2)$$

After finished with the estimation of each block direction, those blocks without significant information on ridges and furrows are discarded based on the following formula:

$$E = \{2(g_x * g_y) + (g_x^2 - g_y^2)\} / W * W * (g_x^2 + g_y^2)$$

For each block, if its certainty level E is below a threshold, then the block is regarded as a background block. The direction map is shown in the following diagram. We assume there is only one fingerprint in each image.

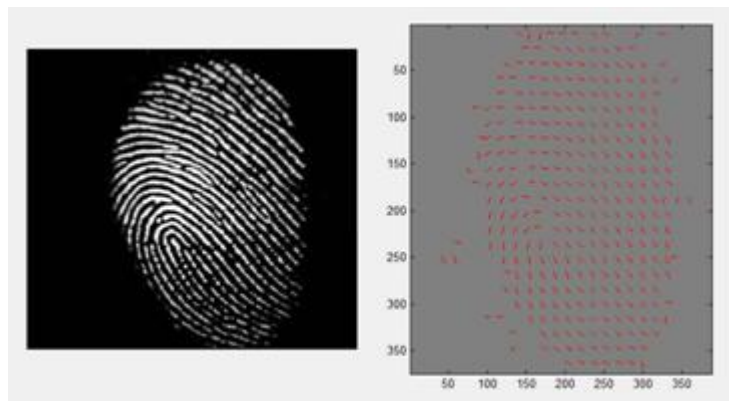


FIGURE 9: Direction map Binarized fingerprint (left), Direction map (right)

- b) **ROI extraction by Morphological operation:** Two Morphological operations called ‘OPEN’ and ‘CLOSE’ are adopted. The ‘OPEN’ operation can expand images and remove peaks introduced by background noise. The ‘CLOSE’ operation can shrink images and eliminate small cavities.



FIGURE 10: Region of Interest

Figure 10 shows the interest fingerprint image area and its bound. The bound is the subtraction of the closed area from the opened area. Then the algorithm throws away those leftmost, rightmost, upper most and bottom blocks out of the bound so as to get the tightly bounded region just containing the bound and inner area.

V. MINUTIA POST-PROCESSING

The procedure of removing false minutia:

1. If the distance between one bifurcation and one termination is less than D and the two minutia are in the same ridge (m1 case) . Remove both of them. Where D is the average inter-ridge width representing the average distance between two parallel neighboring ridges.
2. If the distance between two bifurcations is less than D and they are in the same ridge, remove the two bifurcations. (m2, m3 cases).
3. If two terminations are within a distance D and their directions are coincident with a small angle variation. And they suffice the condition that no any other termination is located between the two terminations. Then the two terminations are regarded as false minutia derived from a broken ridge and are removed. (case m4, m5, m6).
4. If two terminations are located in a short ridge with length less than D , remove the two terminations (m7).

My proposed procedures in removing false minutia have two advantages. One is that the ridge ID is used to distinguish minutia and the seven types of false minutia are strictly defined comparing with those loosely defined by other methods. The second advantage is that the order of removal procedures is well considered to reduce the computation complexity. It surpasses the way adopted by [12] that does not utilize the relations among the false minutia types. For example, the procedure3 solves the m4, m5 and m6 cases in a single check routine and after procedure 3, the number of false minutia satisfying the m7 case is significantly reduced.

VI. MINUTIA MATCH

Given two sets of minutia of two fingerprint images, the minutia match algorithm determines whether the two minutia sets are from the same finger or not an alignment-based match algorithm partially derived from the [14] is used in my replace. It includes two consecutive stages:

Stage 1: Alignment Stage

The ridge associated with each minutia is represented as a series of x -coordinates $(x_1, x_2 \dots x_n)$ of the points on the ridge. A point is sampled per ridge length L starting from the minutia point, where the L is the average inter-ridge length. And n is set to 10 unless the total ridge length is less than $10 * L$. So the similarity of correlating the two ridges is derived from:

$S = \frac{m_{i=0} x_i X_i}{[m_{i=0} x_i^2 X_i^2]^{0.5}}$ Where, $(x_i \sim x_n)$ and $(X_i \sim X_N)$ are the set of minutia for each fingerprint image respectively and m is minimal one of the n and N value.

Stage 2: Match Stage

The matching algorithm for the aligned minutia patterns needs to be elastic since the strict match requiring that all parameters (x, y) are the same for two identical minutia is impossible due to the slight deformations and inexact quantization of minutia. My approach to elastically match minutia is achieved by placing a bounding box around each template minutia. If the minutia to be matched is within the rectangle box and the direction discrepancy between them is very small, then the two minutia are regarded as a matched minutia pair. Each minutia in the template image either has no matched minutia or has only one corresponding minutia. The final match ratio for two fingerprints is the number of total matched pair over the number of minutia of the template fingerprint. The score is $100 * \text{ratio}$ and ranges from 0 to 100. If the score is larger than a pre-specified threshold, the two fingerprints are from the same finger. However, the elastic match algorithm has large computation complexity and is vulnerable to spurious minutia.

VII. EXPERIMENTATION RESULTS

A fingerprint database from the FVC2000 (Fingerprint Verification Competition 2000) is used to test the experiment performance. My program tests all the images without any fine-tuning for the database. The experiments show my program can differentiate imposturous minutia pairs from genuine minutia pairs in a certain confidence level. Furthermore, good experiment designs can surely improve the accuracy as declared by [10] further studies on good designs of training and testing are expected to improve the result.

Here is the diagram for Correct Score and Incorrect Score distribution:

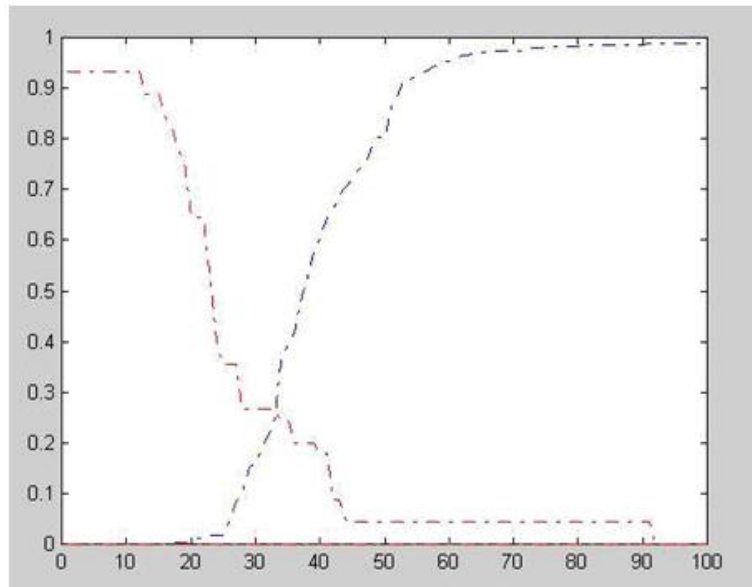


FIGURE 11: Distribution of Correct Scores and Incorrect Scores, Red line: Incorrect Score Green line: Correct Scores

It can be seen from the above figure that there exist two partially overlapped distributions. The Red curve whose peaks are mainly located at the left part means the average incorrect match score is 25. The green curve whose peaks are mainly located on the right side of red curve means the average correct match score is 35. This indicates the algorithm is capable of differentiate fingerprints at a good correct rate by setting an appropriate threshold value.

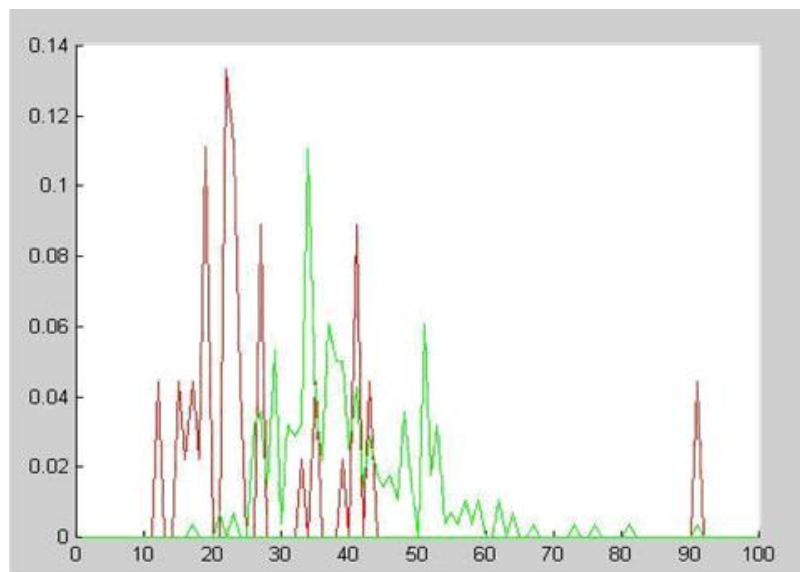


FIGURE 12: FAR and FRR curve, Blue dot line: FRR curve, Red dot line: FAR curve

The above diagram shows the FRR and FAR curves. At the equal error rate of 25%, the separating score 33 will falsely reject 25% genuine minutia pairs and falsely accept 25% imposturous minutia pairs and has 75% verification rate. The high incorrect acceptance and false rejection are due to some fingerprint images with bad quality and the vulnerable minutia match algorithm.

VIII. CONCLUSION

This research has combined many methods to build a minutia extractor and a minutia matcher. The combination of multiple methods comes from a wide investigation into the research paper. Also, some novel changes like segmentation using Morphological operations, minutia marking with special considering the triple branch counting, minutia unification by decomposing a branch into three terminations, and matching in the unified x-y coordinate system after a two-step transformation are used in my replace, which are not reported in other literature I referred to. Also, a program coding with

MATLAB going through all the stages of the fingerprint recognition is built. It is helpful to understand the procedures of fingerprint recognition and demonstrate the key issues of fingerprint recognition.

REFERENCES

- [1] S. Sanderson, J. Erbetta. Authentication for secure environments based on iris scanning technology. IEE Colloquium on Visual Biometrics, 2000.
- [2] D.Maio and D. Maltoni. Direct gray-scale minutiae detection in fingerprints.IEEE Trans. Pattern Anal. And Machine Intell., 19(1):27-40, 1997.
- [3] Jain, A.K., Hong, L., and Bolle, R.(1997), "On-Line Fingerprint Verification," IEEE Trans. On Pattern Anal and Machine Intell, 19(4), pp. 302-314.
- [4] N. Ratha, S. Chen and A.K. Jain, "Adaptive Flow Orientation Based Feature Extraction in Fingerprint Images", Pattern Recognition, Vol. 28, pp. 1657-1672, November 1995.
- [5] Alessandro Farina, ZsoltM.Kovacs-Vajna, Alberto leone, Fingerprint minutiae extraction from skeletonized binary images, Pattern Recognition, Vol.32, No.4, pp877-889, 1999.
- [6] Lee, C.J., and Wang, S.D.: Fingerprint feature extration using Gabor filters, Electron. Lett., 1999, 35, (4), pp.288-290.
- [7] M. Tico, P.Kuosmanen and J.Saarinen. Wavelet domain features for fingerprint recognition, Electroni. Lett., 2001, 37, (1), pp.21-22.
- [8] L. Hong, Y. Wan and A.K. Jain, "Fingerprint Image Enhancement: Algorithms and Performance Evaluation", IEEE Transactions on PAMI ,Vol. 20, No. 8, pp.777-789, August 1998.
- [9] L.C. Jain, U.Halici, I. Hayashi, S.B. Lee and S.Tsutsui. Intelligent biometric techniques in fingerprint and face recognition. 1999, the CRC Press.
- [10] M. J. Donahue and S. I. Rokhlin, "On the Use of Level Curves in Image Analysis," Image Understanding, VOL. 57, pp 652 - 655, 1992.

Kalman Filter Based Approach of a signal by removing ICI for OFDM Channel

Mr. Lokesh Kumar^{1*}, Dr. Javed Khan Bhutto², Mr. Gautam Pandit³

¹M.Tech Scholar, Digital Communication, Marudhar Engineering College, Bikaner.

²Principal & HOD, Department of EE, Marudhar Engineering College, Bikaner.

³M.Tech coordinator, Department of ECE, Marudhar Engineering College, Bikaner.

Abstract— This paper deals with the case of a high speed mobile receiver operating in an orthogonal-frequency division multiplexing (OFDM) communication system. The OFDM communication is very much inspired from the channel frequencies over the network. In such network some kind of orthogonal distortion occurs over the channel called Inter carrier Interference. Here we will improve the ICI using Kalman Filtering improved by using repetitive slot and correlated channel tap.

The proposed work of this paper is when data travel over some channel it suffers from the problem of interference. The interference results the high signal to noise ratio as well as high bit error rate. The proposed system will improved the signal by removing the different kind of impurities over the signal. These impurities include the ICI, PAPR and the noise over the signal. The signal will be more effective than standard OFDM. So we needn't many pilot symbols in practice, still can ensure the algorithm performance and reduce the time- delay and complexity of this algorithm.

Keywords— Kalman Filter, OFDM Channel, mobile receiver, repetitive slot, interference, signal to noise ratio.

I. INTRODUCTION

ORTHOGONAL frequency division multiplexing (OFDM) is an effective technique for high bit-rate transmission. In mobile communications, high speeds of terminals cause Doppler effects that could seriously affect the performance. In such case, dynamic channel estimation is needed, because the radio channel is frequency selective and time-varying, even within one OFDM symbol. It is thus preferable to estimate channel by inserting pilot tones, called comb-type pilots, into each OFDM symbol. Orthogonal frequency division multiplexing (OFDM) is a multicarrier modulation (MCM) technique which seems to be an attractive candidate for fourth generation (4G) wireless communication systems. OFDM offer high spectral efficiency, immune to the multipath delay, low inter-symbol interference (ISI), immunity to frequency selective fading and high power efficiency. However OFDM system suffers from serious problem of high PAPR. In OFDM system output is superposition of multiple sub-carriers. In this case some instantaneous power output might increase greatly and become far higher than the mean power of system. To transmit signals with such high PAPR, it requires power amplifiers with very high power scope. These kinds of amplifiers are very expensive and have low efficiency-cost. If the peak power is too high, it could be out of the scope of the linear power amplifier. This gives rise to non-linear distortion which changes the superposition of the signal spectrum resulting in performance degradation. If no measure is taken to reduce the high PAPR, MIMO-OFDM system could face serious restriction for practical applications. PAPR can be described by its complementary cumulative distribution function (CCDF). In this probabilistic approach certain schemes have been proposed by researchers. These include clipping, coding and signal scrambling techniques. Under the heading of signal scrambling techniques there are two schemes included.

OFDM represents a different system design approach. It can be thought of as a combination of modulation and multiple-access schemes that segments a communications channel in such a way that many users can share it. Whereas TDMA segments are according to time and CDMA segments are according to spreading codes, OFDM segments are according to frequency. It is a technique that divides the spectrum into a number of equally spaced tones and carries a portion of a user's information on each tone. A tone can be thought of as a frequency, much in the same way that each key on a piano represents a unique frequency. By allowing the tones to overlap, the overall amount of spectrum required is reduced.

II. POLYNOMIAL MODELING IN MIMO OFDM SYSTEM

In wireless communication especially in MIMO system the channel modeling is the key area and needs great effort. The main objective of MIMO technology is to increase capacity which is depending on decorrelation properties between antennas and the full rankness of the channel matrix. To fully understand channel behaviour and then we extract formula which represents the channel and to determine the impact of the propagation parameters on the capacity of the channel.

Good channel modeling clearly put the following points:

- It is exactly put the capacity of outdoor and indoor MIMO channel.
- Identifies the important parameters governing capacity.
- Put very simplify conditions to get full rank.

In MIMO systems, a transmitter sends multiple streams by multiple transmit antennas. The transmit streams go through a matrix channel which consists of multiple paths between multiple transmit antennas at the transmitter and multiple receive antennas at the receiver. Then, the receiver gets the received signal vectors by the multiple receive antennas and decodes the received signal vectors into the original information. Here MIMO system model:

$$\mathbf{Y} = \mathbf{H}\mathbf{X} + \mathbf{G} \quad (1)$$

Where \mathbf{Y} and \mathbf{X} are receive and transmit vectors, \mathbf{H} and \mathbf{G} are the channel matrix and noise vector, respectively.

A 3×3 channel matrix is given by

$$\mathbf{H} = \begin{pmatrix} \mathbf{h}_{11} & \mathbf{h}_{12} & \mathbf{h}_{13} \\ \mathbf{h}_{21} & \mathbf{h}_{22} & \mathbf{h}_{23} \\ \mathbf{h}_{31} & \mathbf{h}_{32} & \mathbf{h}_{33} \end{pmatrix}$$

III. OFDM SYSTEM MODEL

A baseband OFDM signal can be represented by [1]

$$b(t) = \sum_{i=1}^{N-1} A_i \cos(\omega_i t + \phi_i)$$

Where A_i is the amplitude, $\omega_i = 2\pi f_i$ is the angular frequency, ϕ_i is the phase of the i^{th} sub-carrier, and N is the number of sub-carriers. According to the modulation technique to be used, either A or ϕ is determined by the data. Now, the baseband OFDM signal $b(t)$ is modulated next, onto a RF carrier with frequency f_c :

$$\begin{aligned} s(t) &= 2b(t)\cos\omega_c t \\ &= 2\sum_{i=0}^{N-1} A_i \cos(\omega_i t + \phi_i) \cos\omega_c t \\ &= \sum_{i=0}^{N-1} A_i \left\{ \cos[(\omega_c + \omega_i)t + \phi_i] + \cos[(\omega_c - \omega_i)t - \phi_i] \right\} \end{aligned}$$

where $\omega_c = 2\pi f_c$, and we assume the phase of the carrier to be zero for simplicity. Since a single side band transmission is enough to carry the information in A_i or ϕ_i , it is assumed that the upper sideband is used, and therefore the transmitted signal can be represented as

$$s(t) = \sum_{i=0}^{N-1} A_i \cos[(\omega_c + \omega_i)t + \phi_i]$$

In this section the theoretical analysis of the effects of frequency errors is presented. The maximum Doppler shift occurs when the two mobile nodes move toward each other, given by [6]

$$f_d = \frac{v f_c}{c}$$

Where v is the relative speed of the two nodes, f_c is the carrier frequency and c is the speed of light (3×10^8 ms). An OFDM signal consists of numerous sub-carriers with different frequencies. The amount of Doppler shift affecting the i^{th} sub-carrier is given by [7].

$$(f_c \pm f_i) \longrightarrow (1 + \xi)(f_c \pm f_i)$$

where ξ is the percentage of the change in frequency and is determined by

$$\xi = \frac{f_d}{f} = \frac{v}{c} \cos \theta$$

The right-hand side of Equation can be written as

$$(1 + \xi)(f_c \pm f_i) = (1 + \xi) f_c \pm (1 + \xi) f_i$$

Which demonstrates that the Doppler frequency shift affects the carrier frequency and the sub-carrier frequencies by the same percentage ξ . The Doppler shift of the carrier frequency can be calculated as

$$f_{dc} = \frac{vf_c}{c} \cos \theta$$

and the Doppler shift of the sub-carrier frequencies as

$$f_{di} = \frac{vf_i}{c} \cos \theta$$

By using Equation again, the transmitted OFDM signal with Doppler shift can be written as

$$s(t) = \sum_{i=0}^{N-1} A_i \cos[(1 + \xi)(\omega_c + \omega_i)t + \phi_i]$$

$$= \sum_{i=0}^{N-1} \{ A_i \cos[(1 + \xi)\omega_i t + \phi_i] \cos[(1 + \xi)\omega_c t] - A_i \sin[(1 + \xi)\omega_i t + \phi_i] \sin[(1 + \xi)\omega_c t] \}$$

In Equation, $A_i \cos [(1+\xi) \omega_i t + \phi_i]$ can be thought of as the envelope of the carrier, $\cos [(1+\xi) \omega_c t]$, which helps to demonstrate that the Doppler shift affects the envelope and the carrier frequency by the same percentage. The Doppler shift also affects the symbol rate and the time synchronization.

3.1 Design of An OFDM System :

The design of an OFDM system requires a trade-off between various parameters as like in all communication system design. Usually, the input parameters to the design are the bit rate, available bandwidth and the maximum delay spread introduced by the channel. The design involves calculation of symbol duration, guard time, number of sub-carriers and the modulation and coding schemes among others.

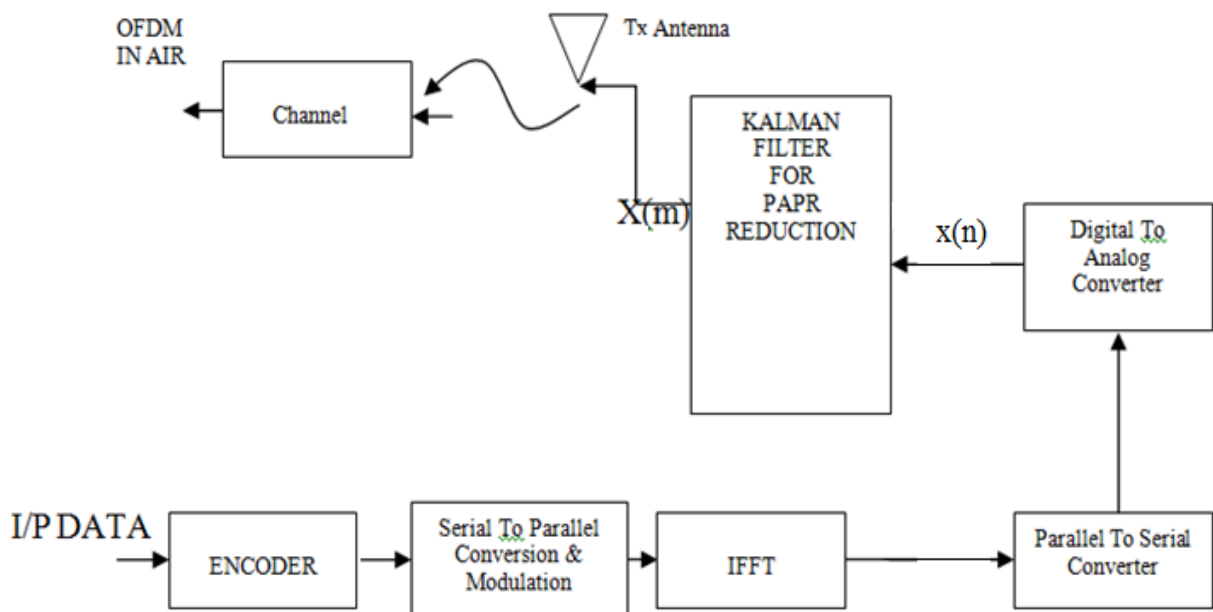


FIGURE 1: Block Diagram of OFDM Transmitter

IV. KALMAN FILTER

Kalman filter is basically designed as a generalized solution to the common problem. It is about to estimate the state of discrete time controlled process by using the basic concept of differential equations. The basic equation followed by Kalman Filter is given as

$$K_k = P_k^- H_k^T (H_k P_k^- H_k^T + V_k R_k V_k^T)^{-1}$$

$$\hat{x}_k = \hat{x}_k^- + K_k \left(z_k - h \left(\hat{x}_k^-, \mathbf{0} \right) \right)$$

$$P_k = (I - K_k H_k) P_k^-$$

V. SIMULATION RESULTS

In this section, we verify the theory by simulation and we Test the performance of the iterative algorithm.

In figure, comparative analysis of PAPR reduction is shown using Kalman Filter. In this work we have implemented a two stage Kalman Filter. The first stage is about to reduce the PAPR. The result shows that the presented approach is more effective with less SNR over the signal.

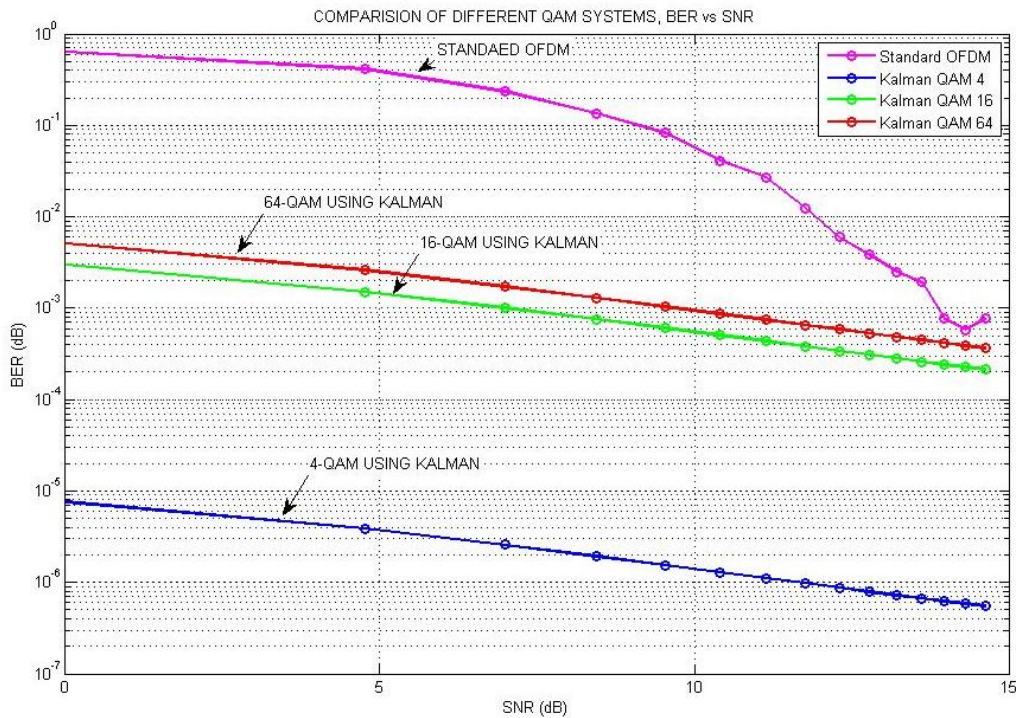


FIGURE 2: Comparison of different QAM Systems, BERvs SNR

When data travel over some channel it suffers from the problem of interference. The interference results the high signal to noise ratio as well as high bit error rate. The proposed system will improved the signal by removing the different kind of impurities over the signal. These impurities include the ICI, PAPR and the noise over the signal. The signal will be more effective than standard OFDM.

VI. CONCLUSION

In this project, the performance of OFDM systems in the presence of frequency offset between the transmitter and the receiver has been studied in terms of the Carrier-to-Interference ratio (CIR) and the bit error rate (BER) performance. Inter-carrier interference (ICI), which results from the frequency offset, degrades the performance of the OFDM system.

One method is explored in this project for mitigation of the ICI i.e. ICI self-cancellation (SC). By using this method the BER is improved in comparison to simple OFDM system.

In this project, the simulations were performed in an AWGN channel. This model can be easily adapted to a flat-fading channel with perfect channel estimation. Performing simulations to investigate the performance of this ICI cancellation schemes in multipath fading channels without perfect channel information at the receiver can do further work.

REFERENCES

- [1] H. Hijazi and L. Ros, "Time-varying channel complex gains estimation and ICI suppression in OFDM systems" in IEEE GLOBAL COMMUNICATIONS Conf., Washington, USA, Nov. 2007.
- [2] H. Hijazi and L. Ros, "Polynomial estimation of time-varying multipath gains with intercarrier interference mitigation in OFDM systems" in IEEE Trans. Vehic. Techno., vol. 57, no. 6, November 2008.
- [3] A. R. S. Bahai and B. R. Saltzberg, Multi-Carrier Dications: Theory and Applications of OFDM: Kluwer Academic/Plenum, 1999.
- [4] M. Hsieh and C. Wei, "Channel estimation for OFDM systems based on comb-type pilot arrangement in frequency selective fading channels" in IEEE Trans. Consumer Electron., vol.44, no. 1, Feb. 1998.
- [5] Z. Tang, R. C. Cannizzaro, G. Leus and P. Banelli, "Pilot-assisted timevarying channel estimation for OFDM systems" in IEEE Trans. Signal Process., vol. 55, pp. 2226-2238, May 2007.
- [6] S. Tomasin, A. Gorokhov, H. Yang and J.-P. Linnartz, "Iterative interference cancellation and channel estimation for mobile OFDM" in IEEE Trans. Wireless Commun., vol. 4, no. 1, pp. 238-245, Jan. 2005.
- [7] B. Yang, K. B. Letaief, R. S. Cheng and Z. Cao, "Channel estimation for OFDM transmisson in mutipath fading channels based on parametric channel modeling" in IEEE Trans. Commun., vol. 49, no. 3, pp. 467-479, March 2001.
- [8] E. Anderson and Z. Bai, LAPACK User's Guide: Third Edition,SIAM, Philadelphia, 1999.
- [9] Wikipedia contributors,"Linear regression", Wikipedia, The Free Encyclopedia.
- [10] K. E. Baddour and N. C. Beaulieu, "Autoregressive modeling for fading channel simulation" in IEEE Trans. Wireless Commun., vol. 4, no. 4, pp. 1650-1662, July 2005.
- [11] B. Anderson and J. B. Moore, Optimal filtering, Prentice-Hall, 1979.
- [12] W. C. Jakes, Microwave Mobile Communications. Piscataway, NJ: IEEE Press, 1983.



AD Publications

**Sector-3, MP Nagar, Bikaner,
Rajasthan, India**

www.adpublications.org, info@adpublications.org